Annu. Rev. Astron. Astrophys. 2000. 38:613–66


# WINDS FROM HOT STARS

Rolf-Peter Kudritzki and Joachim Puls
*Institut für Astronomie und Astrophysik der Universität München, Scheinerstr. 1, D-81679 München, Germany; e-mail: kud@usm.uni-muenchen.de, uh101aw@usm.uni-muenchen.de*



**Key Words** mass loss, stellar winds, massive stars, Central Stars of Planetary Nebulae, stellar evolution

■ **Abstract** This review deals with the winds from "normal" hot stars such as O-stars, B- and A-supergiants, and Central Stars of Planetary Nebulae with O-type spectra. The advanced diagnostic methods of stellar winds, including an assessment of the accuracy of the determinations of global stellar wind parameters (terminal velocities, mass-loss rates, wind momenta, and energies), are introduced and scaling relations as a function of stellar parameters are provided. Observational results are interpreted in the framework of the stationary, one-dimensional (1-D) theory of line-driven winds. Systematic effects caused by nonhomogeneous structures, time dependence, and deviations from spherical symmetry are discussed. The review finishes with a brief description of the role of stellar winds as extragalactic distance indicators and as tracers of the chemical composition of galaxies at high redshift.

## 1. INTRODUCTION

All hot stars have winds driven by radiation. These winds become directly observable in spectral energy distributions and spectral lines as soon as the stars are above certain luminosity borderlines in the HRD. For massive stars of spectral type O, B, and A, the borderline corresponds to $10^4$ $L_\odot$. Above this threshold in luminosity all massive stars show direct spectroscopic evidence of winds throughout their lifetime (Abbott 1979). An analogous threshold exists for stars of intermediate and low mass ($M_{ZAMS} \leq 8$ $M_\odot$), when they evolve through the post-AGB phases toward the white dwarf final stage. Here, all objects more massive than 0.58 $M_\odot$ or more luminous than $10^{3.6}$ $L_\odot$ exhibit direct signatures of winds in their spectra (Pauldrach et al 1989).

Winds are able to modify the ionizing radiation of hot stars dramatically (see Gabler et al 1989, 1991, 1992; Najarro et al 1996). Their momenta and energies contribute substantially to the dynamics and energetics of the ambient interstellar medium in galaxies or of surrounding gaseous nebulae. Even weak winds (i.e. those with no direct spectroscopic evidence of mass-outflow) may produce

thin gaseous envelopes around stars before they become red supergiants with dense slow winds or explode as supernovae in later stages of their evolution. The gas-dynamical interaction of stellar plasmas streaming with different velocities and densities will then eventually lead to complex surrounding structures directly observable with high spatial resolution. In binary systems, winds can be partially accreted or can produce shocks of colliding winds resulting in X-ray emission in both cases. Winds (*a*) affect the physics of stellar atmospheres by dominating the density stratification and the radiative transfer through the presence of their macroscopic transonic velocity fields, (*b*) substantially influence the evolution of stars by modifying evolutionary timescales, chemical profiles, surface abundances, and stellar luminosities, and (*c*) are vital for the evolution of galaxies by their input of energy, momentum, and nuclear-processed material to the ISM.

In addition, stellar winds are a gift of nature, allowing quantitative spectroscopic studies of the most luminous stellar objects in distant galaxies and, thus, enabling us to obtain important quantitative information about their host galaxies. Broad stellar wind lines can be identified in spectra integrating over the stellar populations of extremely distant galaxies at high redshift even when the spectral resolution and the signal-to-noise ratio are only moderate (Steidel et al 1996). Particularly in cases when the flux from these galaxies is amplified by gravitational lensing through foreground galaxy clusters, stellar wind lines can be used to estimate metallicities of starbursting galaxies in the early universe (Pettini et al 2000). In the local universe, the population synthesis of spectroscopic stellar wind features observed in the integrated light of starbursting regions of galaxies can yield important information about the population of stars formed (Leitherer 1998, Leitherer et al 1999). Finally, the observation of winds of isolated blue supergiants as individuals in spiral and irregular galaxies provides an independent new tool for the determination of extragalactic distances by means of the wind momentum–luminosity relationship (Kudritzki et al 1995, Puls et al 1996, Kudritzki 1998, Kudritzki et al 1999).

In view of the important role of winds from hot stars in so many areas of astrophysics, it is not surprising that the number of papers and conferences dealing with them is enormous. As a result, a complete review covering all aspects in theory and observation is impossible within the framework of this review series, and a restriction of the subject is needed. Therefore, we have restricted this review to the discussion of winds from "normal" hot stars in well-established evolutionary stages such as dwarfs, giants, and supergiants. We do not discuss objects with extreme winds such as Wolf-Rayet stars, luminous blue variables in outburst, Be-stars, etc. We are aware of the fact that by this restriction a significant amount of active research in interesting areas of stellar physics is omitted. On the other hand, it allows us to cover the most fundamental stages of stellar evolution in sufficient depth.

The goal of this review is to inform about the advanced diagnostic methods of stellar winds, including an assessment of the accuracy of the determinations of global stellar wind properties such as terminal velocities, mass-loss rates, wind

momenta, and wind energies (Section 2). Simple empirical scaling relations of these stellar wind properties as a function of stellar parameters is provided (Section 3) and is interpreted in the framework of the stationary, 1-D theory of radiation-driven winds (Section 4). The influence of systematic effects caused by nonhomogeneous structures, time dependence, and deviations from spherical symmetry caused by rotation is discussed (Sections 4 and 5). The review finishes with a brief discussion of stellar wind lines as extragalactic distance indicators and as tracers of chemical composition of galaxies at high redshift, in particular in view of the potential of the new generation of very large ground-based telescopes (Section 6).



## 2. STELLAR PARAMETERS AND GLOBAL WIND PROPERTIES

### 2.1 Global Stellar Wind Parameters

Winds of hot stars are characterized by two global parameters, the terminal velocity $v_\infty$ and the rate of mass loss $\dot{M}$. Because these winds are initiated and then continuously accelerated by the absorption of photospheric photons in spectral lines, the velocity $v_\infty$ reached at very large distances from the star, where the radiative acceleration approaches zero because of the geometrical dilution of the photospheric radiation field, corresponds to the maximum velocity of the stellar wind. If we assume that winds are stationary and spherically symmetric, then the equation of continuity yields at any radial coordinate R in the wind

$$\dot{M} = 4\pi R^2 \rho(R) V(R). \tag{1}$$

$V(R)$ and $\rho(R)$ are the velocity field and the density distribution, respectively. We regard those as local stellar wind parameters. A determination of the global parameters from the observed spectra is only possible with realistic assumptions about the stratification of the local parameters. We discuss this point carefully in the sections below.

From Equation 1 it is evident that the average mass density $\bar{\rho}$ (Equation 2 with $R_*$ the photosperic radius) is another global parameter related to the observability of stellar winds. For instance, the optical depths of a metal resonance line [with a line absorption coefficient $\propto \rho(R)$] or a recombination line such as $H_\alpha$ [with a line absorption coefficient $\propto \rho^2(R)$] are proportional to $Q_{res}$ and $Q^2$, respectively, defined as

$$\bar{\rho} = \frac{\dot{M}}{4\pi R_*^2 v_\infty}, \qquad Q_{res} = 4\pi \bar{\rho} \frac{R_*}{v_\infty}, \qquad Q^2 = (4\pi)^2 \bar{\rho}^2 \frac{R_*}{v_\infty}. \tag{2}$$

In the following we describe the diagnostic methods used to obtain these global parameters.

## 2.2 General Strategy

It is important to realize that the determination of stellar wind properties from observed spectra is never straightforward and simple. Global stellar wind parameters as defined in the previous subsection are not direct observables. Their determination relies on stellar atmosphere models, including the hydrodynamic effects of winds, which form the basis for radiative transfer calculations to be compared with the observations. In other words, whenever we discuss "observations of stellar winds," we must be aware of the fact that those observed stellar wind properties are already the result of diagnostic techniques based on a substantial amount of theoretical modeling. Depending on the degree of sophistication of the underlying model, but also depending on which part of the spectrum is used for the determination of which stellar wind quantity, the reliability of the results obtained can be vastly different.

A few examples may illustrate this point. The determination of the mass-loss rate $\dot{M}$ from a significant "thermal" radio excess in the spectral energy distribution (for details, see discussion in the corresponding subsection) caused by the Bremsstrahlung of the stellar wind envelope requires only a very simple analytical stellar wind model and radiative transfer calculation, because the thermal free-free and bound-free emission of a plasma is a simple process as long as the wind is homogeneous (not clumpy), spherically symmetric, and stationary. Mass-loss rates obtained in this way are usually regarded as sufficiently accurate. However, even such reliable "observations" may be severely affected in a systematic way as soon as winds are clumpy and deviate from spherical symmetry.

In such a situation, an alternative would be the analysis of the P-Cygni profiles of ultraviolet (UV) metal resonance lines. One can show that for these lines the influence of inhomogeneity and clumpiness is less important (see Section 5). However, to deduce $\dot{M}$, one needs an accurate estimate of the element abundance and the degree of ionization of the ion producing the analyzed P-Cygni line. In particular for the latter, a tremendous effort in terms of non-LTE multi-level and multi-line atmospheric modeling is necessary to obtain results (see Pauldrach et al 1994, 1998; Taresch et al 1997; Haser et al 1998), which are still affected by open questions such as the contribution of ionizing radiation from shocks embedded in the stellar wind flow. In consequence, mass-loss rates determined in this way are usually regarded as less reliable.

A discussion of observed global stellar wind parameters, therefore, requires a strategy concerning the underlying atmospheric models used for the diagnostics. On the one hand, for the analysis methods applied, the models have to be sophisticated enough so that the results appear to be reliable; on the other hand, the models have to be simple enough so that a large number of objects can be analyzed and discussed differentially in a parameter space of reasonable dimensions.

As a result of this consideration, the "standard model" for stellar wind diagnostics is rather simple. A stationary, spherically symmetric smooth stellar wind obeying the equation of continuity (Equation 1) is adopted with a velocity field in

the supersonic region of the wind of the form

$$V(R) = v_\infty \left(1 - b\frac{R_*}{R}\right)^\beta, \qquad b = 1 - \left(\frac{V(R_*)}{v_\infty}\right)^{\frac{1}{\beta}}. \tag{3}$$

The constant b fixes the velocity at the inner boundary of the wind to the prespecified value $V(R_*)$, which is usually of the order of the isothermal sound speed. Velocity fields of this form are predicted by the theory of radiation-driven winds (see Castor et al 1975, Pauldrach et al 1986), and their use for stellar wind diagnostics is justified a posteriori by the quality of the line profile fits achieved (cf Section 2.4). $v_\infty$ and $\beta$ are treated as fit parameters to be determined from the spectrum. The selected value of $V(R_*)$ has little influence on the computed spectrum and is of minor importance.

A simple model defined by Equations 1 and 3 is usually sufficient to calculate a UV resonance line or to make a prediction about the emitted flux at radio wavelength. Of course, one additionally needs to specify the electron temperature in the wind and, for the UV diagnostics, the incident radiation field at the inner boundary. For the latter, the photospheric flux is chosen (usually from a photospheric model), and for the former a value equal to or somewhat smaller than the effective temperature of the star is adopted, assuming that the wind is in radiative equilibrium.

Although this simple approach is entirely adequate to analyze UV resonance lines with regard to the velocity field and opacity structure (Section 2.4.1) and radio fluxes with regard to mass-loss rates (Section 2.4.4), a more complex treatment is needed as soon as lines and continua in the optical and infrared are included in the analysis. In these cases, the spectral information usually originates simultaneously from the quasi-hydrostatic photospheric layers below the sonic point and from the stellar wind layers above. As has been demonstrated by Gabler et al (1989), such a situation requires the use of "unified model atmospheres," which has now become the standard treatment for model atmospheres of hot stars with winds. Unified models are stationary, in non-LTE and in radiative equilibrium, they are spherically extended, and they yield the entire sub- and supersonic atmospheric structure, either taking the density and velocity structure from the hydrodynamics of radiation-driven winds or adopting a smooth transition between an outer wind structure, as described by Equations 1 and 3 and by a hydrostatic stratification. They can be used to calculate energy distributions simultaneously with "photospheric" and "wind" lines, and most important, they can treat the multitude of "mixed cases," where a photospheric line is contaminated by wind contributions. This concept turned out to be extremely fruitful for the interpretation of hot star spectra and has led to the rapid development of significant refinements and improvements in parallel by several groups. Basic papers describing the status of the work in the different groups are those by Sellmaier et al (1993), Schaerer & Schmutz (1994), Schaerer & de Koter (1997), Hillier & Miller (1998), Santolaya-Rey et al (1997), Taresch et al (1997), and Pauldrach et al (1994, 1998). For the investigation of global stellar wind parameters from optical spectra or

energy distributions, model atmospheres of this type are preferred (see discussion below).

At this stage, a short comment on the reliability of these "standard wind models" is necessary. It is certainly true that there is significant evidence for nonstationarity, clumpiness, shocks, and deviations from spherical symmetry and radiative equilibrium (see Moffat et al 1994, Kaper & Fullerton 1998, Wolf et al 1999). There are two reasons why these phenomena are ignored in the standard diagnostics. First, the amplitudes of deviations from the smooth stationary model used are normally not very large [even in the cases where spectral variability looks dramatic (see Kudritzki 1999a)], thus the standard analysis is thought to yield reliable average models of the stellar winds. Second, for obvious reasons, the appropriate inclusion of deviations from the standard model requires a significant additional effort in the diagnostics and a development of new radiative transfer methods, a task not yet completed. A discussion of the possible effects is given in Sections 4 and 5.



## 2.3 Stellar Parameters from Photospheric Diagnostics

To discuss the physical connection of global stellar wind parameters with the stellar properties, one needs an estimate of the stellar parameters, such as effective temperature $T_{\rm eff}$, luminosity $L$, photospheric radius $R_*$, gravity $\log g$, chemical composition, etc. There are two ways to proceed. The first is to adopt general calibrations of effective temperature and bolometric correction with spectral type and to determine $L$, $R_*$, and $T_{\rm eff}$ from de-reddened photometry, distance, and spectral type. The stellar mass follows then from a comparison with evolutionary tracks in the HRD.

The second and more accurate way relies on model atmospheres to determine $T_{\rm eff}$ and $\log g$ as the most fundamental atmospheric parameters by fitting simultaneously two sets of spectral lines, one depending mostly on $T_{\rm eff}$ and the other on $\log g$. For the former, one uses line profiles of different ionization stages ("ionization equilibrium") and for the latter the higher (less wind-contaminated) Balmer lines. Fit curves in the ($\log g$, $\log T_{\rm eff}$)-plane along which the calculated line profiles of the two different sets agree with the observations then yield effective temperature and gravity, together with an estimate of the uncertainties. For O-stars, the HeI/II ionization equilibrium is normally used (Kudritzki 1980; Simon et al 1983; Bohannan et al 1986; Voels et al 1989; Kudritzki et al 1983, 1992; Herrero et al 1992, 1999), which is also applied in the case of very early B-supergiants (Lennon et al 1991, McErlean et al 1998). For B-supergiants of later spectral type, $T_{\rm eff}$ is obtained from the SiII/III/IV ionization equilibrium (McErlean et al 1999), and for A-supergiants the MgI/II equilibrium has proven to be reliable (Venn 1995, 1999; McCarthy et al 1995, 1997). The model atmosphere approach will also yield the chemical composition of the stars from a fit of the complete line spectrum (see references above; see also Taresch et al 1997, Haser et al 1998). Using the distance modulus, the stellar radius is then obtained from the model atmosphere flux and de-reddened photometry, which then yields the luminosity. The stellar mass follows from radius and gravity.

A few problems with this approach need to be discussed. Herrero et al (1992) in their quantitative spectroscopic study of a large sample of galactic O-stars detected a systematic "mass discrepancy." They found that for evolved O-stars approaching the Eddington-limit, the stellar masses derived from evolutionary tracks and stellar luminosities are significantly larger than the masses obtained from spectroscopic gravities. Which masses are correct is still an open question. The most recent calculations by Langer & Heger (1998), Maeder (1998), and Meynet (1998) indicate that stellar evolution, including rotation and rotationally induced interior mixing, would enhance the luminosity significantly for any given mass. In addition, enhanced mass loss along the evolutionary track would further reduce the mass and bring the evolutionary masses into agreement with the spectroscopic and wind masses (Langer et al 1994). On the other hand, because Herrero et al used hydrostatic non-LTE models in their study and neglected wind contamination of the hydrogen and helium lines (Gabler et al 1989, Sellmaier et al 1993, Puls et al 1996), their spectroscopic masses may have been systematically underestimated. In addition, the neglect of metal line blanketing in their analysis could have caused a small effect (see Lanz et al 1996; but see also Hubeny et al 1998).

It is important to note here that this uncertainty of stellar mass depending systematically on the approach used for the mass determination will introduce a systematic effect in the relationship between terminal stellar wind velocity and escape velocity from the stellar photosphere discussed in Section 3.

Another systematic uncertainty affects the effective temperature of O-stars at the earliest spectral types (O3 and O4), which in the classical work (see references above) relies on the strength of one single, very weak He I line ($\lambda$4471). Blanketing (Hubeny et al 1998), but also such exotic effects as noncoherent electron scattering of He II resonance lines in the EUV (extreme ultra-violet) (see Santolaya-Rey et al 1997), may have significant influence on this line. The introduction of new effective temperature indicators for these objects, such as metal lines in the optical and UV, leads to results that are contradictory at the moment (see de Koter et al 1998; but see also Taresch et al 1997, Pauldrach et al 1994). For a determination of the luminosity of these objects, a careful investigation of this aspect is urgently needed.

A third important uncertainty concerns the helium abundance of late O- and B-supergiants. The work by Lennon et al (1991) and Herrero et al (1992) led to the conclusion that the helium abundance in the atmospheres of such stars is significantly enhanced, indicating the presence of CNO-processed material mixed from the stellar interior. Although evolutionary tracks with rotational mixing support this result (see references above), recent analyses by Smith & Howarth (1998) and McErlean et al (1998) indicate that the helium enhancement is probably much smaller if the non-LTE radiative transfer calculations include the effect of photospheric microturbulence of the order of 10 km/s in the rate equations. The problem is not completely solved at the moment and needs further investigation. For the determination of effective temperatures and mass-loss rates, this uncertainty may turn out to be important (see Section 3).

An interesting new route to determine stellar parameters is infrared (IR) spectroscopy. Pioneering IR spectral classification work by Hanson and colleagues (1994, 1996, 1997) has demonstrated that K-band spectroscopy allows the determination of spectral type and luminosity class and, therefore, the determination of effective temperature and gravity in such completely analogous ways as optical spectroscopy. This new technique proves to be extremely valuable for massive hot stars embedded in highly dust-obscured regions of star formation, such as ultracompact or normal HII regions (Hanson 1998, Conti & Blum 1998, Drew 1998) or in the galactic center (Najarro et al 1994, 1997; Figer et al 1998). Its impact on the determination of global stellar wind parameters is discussed in Section 2.4.3.



## 2.4 Stellar Wind Diagnostics

In principle, two types of lines are formed in a stellar wind: P-Cygni profiles, with a blue absorption trough and a red emission peak; and pure emission profiles or absorption lines refilled by wind emission. The difference is caused by the reemission process after the photon has been absorbed within the line transition.

If the photon is immediately reemitted by spontaneous emission, then we have the case of line scattering with a source function proportional to the geometrical dilution of the radiation field (optically thin case) or an even steeper decline (roughly $\propto r^{-3}$, optically thick case), and a P-Cygni profile will result.

If the reemission occurs as a result of a different atomic process, for instance after a recombination of an electron into the upper level, after a spontaneous decay of a higher level into the upper level or after a collision, then the line source function will possibly not dilute and may stay roughly constant as a function of radius so that an emission line (or an absorption line weaker than formed by purely photospheric processes) results.

Typical examples for P-Cygni profiles are UV resonance transitions connected to the ground level, whereas excited lines of an ionization stage into which frequent recombination from higher ionization stages occurs will produce emission lines, as is the case, e.g., for $H_\alpha$ in O-supergiants.

Both types of lines can be used in principle to determine $\dot{M}$, $v_\infty$, and the shape of the velocity law $\beta$. The advantages and constraints of the different methods are discussed in the following, as are the diagnostic possibilities related to continuous wind emission in the IR and radio domain.

### 2.4.1 UV Resonance and Subordinate Lines

The specific shape of typical UV P-Cygni profiles in hot stars (e.g. from the resonance lines of CIV, NV, SiIV, OVI, etc) (see Walborn et al 1985) can be explained as follows. The profile consists of two components: Because of its interaction with wind material in front of the stellar disk, photospheric radiation is scattered out of the observer's line of sight, and an absorption trough is formed. Because the material is moving toward the observer, the absorption is blueshifted (from zero to a frequency corresponding to some maximum velocity; see below). Superimposed

onto the absorption trough is the second component, an emission profile that is formed in the wind lobes and again in front of the disk. This wind emission consists of photons that have been absorbed previously and are scattered into the observer's line of sight. Because the reemission occurs in both hemispheres of the wind (positive and negative projected velocities!), the corresponding profile is almost symmetrical with respect to line center. Note, however, that the wind emission from material behind the photospheric disk is not visible ("occulted region"). Consequently, the symmetry is slightly distorted, and the emission profile on the red side is weaker than on the blue one. By adding the blue absorption trough and the emission profile, the typical shape of a P-Cygni line is readily understood.

P-Cygni lines are usually analyzed by means of the so-called SEI method (Sobolev plus exact integration; cf Lamers et al 1987), which is based on the notion (Hamann 1981a) that the profile of such a line can be simulated with high precision if the source functions of the components (usually two due to fine-structure splitting of the lower or upper level) are calculated in the Sobolev approximation (for details, see Sobolev 1957, Castor 1970) and only the "formal integral" is done exactly, i.e. accounting for the finite profile width. For purely scattering singlets then, the source function is given by the ratio of "core penetration" to total "escape probability" (Castor 1970), with straightforward generalizations in the case of doublet formation (Hamann 1981a, Olson 1982, Puls 1987, Lamers et al 1987).

The crucial quantity that controls the line formation process (both with respect to absorption as well as for defining the escape probabilities) is the Sobolev optical depth of the specified line,

$$\tau_{\rm S}(r) = \frac{\bar{\chi}(r) R_* \lambda}{v_\infty {\rm d}v/{\rm d}r}; \qquad \bar{\chi}(r) = \frac{\pi e^2}{m_{\rm e} c} f n_{\rm l}(r). \tag{4}$$

$\bar{\chi}$ is the frequency integrated line opacity, $\lambda$ the wavelength, $f$ the oscillator-strength, and $n_{\rm l}$ the lower occupation number of the transition, neglecting stimulated emission. Here and in the following, $r$ is the radius in units of stellar radius $R_*$ and $v(r)$ the velocity in units of terminal velocity $v_\infty$.

It is important to understand that the line optical depth in expanding atmospheres or winds has an entirely different character than in hydrostatic photospheres. In winds, the interaction photon/absorbing atom is restricted to a geometrically very narrow region of thickness $\Delta r = v_{\rm th}(v_\infty {\rm d}v/{\rm d}r)$ (the Sobolev length). Thus, optical depth is a local quantity in stellar winds, described to a good approximation by Equation 4. By expressing the occupation number in terms of local density $\rho = \dot{M}/(4\pi R_*^2 r^2 v_\infty v)$, this quantity is given by

$$\tau_{\rm S}(r) = \frac{k(r)}{r^2 v {\rm d}v/{\rm d}r}; \qquad k(r) = E(r) X(r) \frac{\dot{M}}{R_* v_\infty^2} \frac{(\pi e^2)/(m_{\rm e} c)}{4\pi m_{\rm H}} \frac{A_k}{1 + 4 Y_{\rm He}} f\lambda, \tag{5}$$

if $E$ is the excitation factor of the lower level, $X$ the ionization fraction, $A_{\rm k}$ the abundance of the element with respect to hydrogen, and $Y_{\rm He}$ the helium abundance.

From the above equation, it is obvious that the appropriate scaling quantity is given by $\dot{M}/(R_* v_\infty^2) = Q_{\rm res}$ (Equation 2), as long as the ionization fraction has no external $\rho$ dependence, i.e. as long as the ground-state occupation follows the density stratification.

Because we have assumed a velocity law of the form $V(r) = v_\infty(1 - b/r)^\beta$ (cf Section 2.2), the quantities that can be derived at maximum by a fit to observed P-Cygni lines are $v_\infty$, $\beta$, and $k(r)$, so that, for known helium abundance, the information with respect to mass loss shows up only in the product $E(r)X(r)A_{\rm k}\dot{M}/R_*$. In consequence, mass-loss rates can be determined from P-Cygni lines only if the ionization/excitation fraction (as function of radius or a mean value; see below) of the specified ion/level is known as well as the abundance!

***Saturated Profiles*** Saturated profiles are often found for CIV, NV in early O-stars and SiIV in late O-supergiants and are related to a large optical depth $\tau_{\rm S} \geq 3$ everywhere in the wind. In contrast to photospheric profiles, this condition can be more easily achieved for wind lines due to their additional dependence on the velocity gradient $\mathrm{d}v/\mathrm{d}r$ (Equation 4). For lines with a rather constant ionization/excitation fraction throughout the wind, the variation of line optical depth depends only on the steepness of the velocity law,

$$\tau_{\rm S} \propto (r^2 v \mathrm{d}v/\mathrm{d}r)^{-1} \propto v(r)^{\frac{1}{\beta}-2}. \qquad (6)$$

For typical O-star values, $\beta = 0.7 \ldots 1.5$ (see below), the variation is only mild, of the order of 10–100 in the region between the sonic point and infinity. In consequence, if a line has a large optical depth in the sonic region, the chances are good that this is also the case throughout the wind.

The absorption trough of such a saturated profile shows nearly zero intensity for all frequencies corresponding to velocities $v = 0 \ldots v_\infty$, and the profile shape depends exclusively on the emission profile, i.e. on the source function in the optically thick case. As can be easily shown, however, for large optical depths this quantity depends only on the velocity field (with an asymptotic behavior $\propto r^{-3}$), because the aforementioned ratio of escape probabilities becomes independent of line opacity, i.e independent of any information concerning occupation numbers. Consequently, saturated profiles allow in principle an easy measurement of terminal velocities from the frequency position of the blue absorption edge as well as a determination of $\beta$ from the shape of the emission peak; however, only upper limits for the product of $(E X A_{\rm k}\dot{M}/R_*)$ are possible.

Figure 1 gives an example for the determination of $v_\infty$ by this method. High-precision measurements with an accuracy of 5% can be obtained in this way (for details and related methods, see Hamann 1981a,b; Lamers et al 1987; Groenewegen & Lamers 1989; Howarth & Prinja 1989; Groenewegen et al 1989; Haser et al 1995; Haser 1995), and typical values $\beta = 0.7 \ldots 1.5$ are found for OB-stars with supergiants having a clear tendency toward higher $\beta$. For A-supergiants, values as high as $\beta = 3 \ldots 4$ can be found (Stahl et al 1991) (Section 2.4.2).

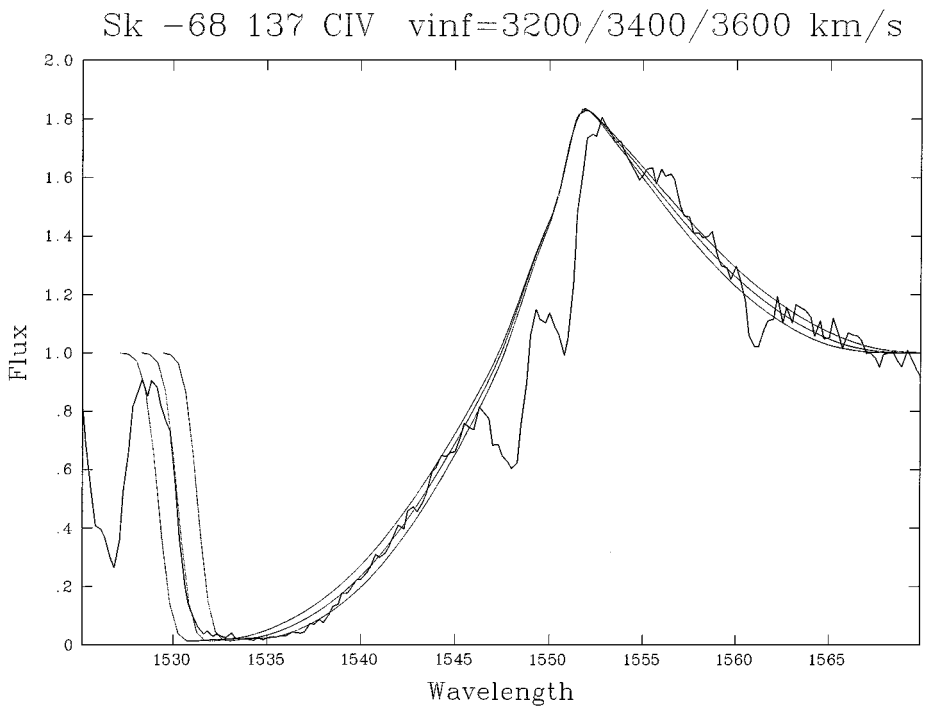


**Figure 1** Radiative transfer calculations for the saturated ultraviolet CIV resonance doublet in the HST FOS spectrum of the large Magallanic cloud O3-star Sk-68° 137 for three different values (3200, 3400, and 3600 km/s) of $v_\infty$. From Kudritzki (1998).

***Unsaturated Profiles*** Unsaturated profiles arise when $\tau_S$ becomes of the order of unity or smaller somewhere in the wind and decent diagnostics concerning $k(r)$ or $k(v)$ (Equation 5), respectively, are possible in the corresponding region: Both the depth and shape of the absorption trough as well as of the emission component [with source function(s) $\propto r^{-2}$] become dependent on line opacity. Note, however, that in this case, the terminal velocity can no longer be determined because the absorption extends only to a certain maximum velocity $<v_\infty$. Additionally, the deduction of $\beta$ becomes impossible because of the intrinsic coupling of ionization fraction and velocity law in the definition of $\tau_S$. In order to derive a unique solution for $k(v)$, the parameters $v_\infty$ and $\beta$ have to be derived independently, e.g. from saturated profiles.

Line fits to unsaturated profiles can be obtained by either parameterizing the optical depth as a function of velocity (Lamers et al 1987, Groenewegen & Lamers 1989), by parameterizing the run of $k(v)$ (Hamann 1981a), or by a parameter-free analysis based on a Newton-Raphson method (Haser et al 1994, Haser 1995). Despite the impressive quality of those fits, their diagnostical value with respect

to $\dot{M}$ is marginal because the ionization fractions have to be predescribed and depend on complicated details of theoretical model computations (cf Section 2.2). In addition, a rather precise determination of the element abundances is needed.

Recently, however, Lamers et al (1999a) have suggested a significant improvement with respect to this dilemma: For unsaturated lines, it is easy to derive the column density of absorbers between velocities $v_1$ and $v_2$ from the actual fit quantity $\tau_S(v)$ itself, as well as the product of a mean ionization/excitation factor $\langle q_k \rangle$ with $\dot{M}A_k/R_*$ in dependence of this column density (cf Howarth & Prinja 1989). Extensive tables of column densities and products of $(\dot{M}\langle q_k \rangle)$ for large samples of O-stars have been determined by Howarth & Prinja (1989) (pure Sobolev analysis) and Haser (1995).

If these data are now combined with independent determinations of mass-loss rates (and abundances and stellar radii are known with reasonable accuracy), empirical mean ionization factors $\langle q_k \rangle$ can be determined. Lamers et al (1999) used the results from the UV diagnostic studies by Groenewegen & Lamers (1989) and Haser (1995), in conjunction with the latest results for mass-loss rates from $H_\alpha$ (Section 2.4.2) and thermal radio emission (Section 2.4.4), and derived empirical ionization/excitation fractions for all relevant UV transitions for selected O-stars covering the complete domain of spectral types and luminosity classes. Introducing calibrations of $\langle q_k \rangle$ with effective temperature, it should then be possible to derive mass-loss rates from UV profiles alone in future investigations (e.g. from FUSE spectra), provided the abundances are known. In agreement with earlier results by Haser (1995), Lamers et al (1999a) showed that SiIV is best suited for this kind of approach.

Even earlier, it was pointed out by Walborn & Panek (1984) that this line can be used as an indicator for the stellar luminosity, an effect theoretically explained by Pauldrach et al (1990) that relates to the fact that SiIV is always a trace ion in the O-star domain, with SiV (inert gas configuration) being the dominant ion. Thus, by means of a simplified non-LTE argumentation (e.g. Abbott 1982), it is easy to show that $X(r)$ has an explicit dependence proportional to density, namely $X \propto n_e/W$ with electron-density $n_e$ and dilution factor $W$. For smooth winds, then, $X(v) \propto \bar{\rho}/v$ and $k(v)$ scales with $Q^2$ instead of $Q_{res}$. This increases the sensitivity of SiIV both with respect to $\dot{M}$ (see above) as well as with luminosity, anticipating the tight coupling of mass loss with luminosity in radiatively driven winds (Section 3 and 4). Note finally that the scaling of SiIV resembles that of $H_\alpha$ discussed in the next subsection.

***Problems*** By means of the discussed line fits, precise "measurements" of $v_\infty$, $\beta$, $v_{turb}$, and column densities are possible, at least as long as one of the strategic lines is saturated and the contamination of unsaturated profiles with lines formed already in the photosphere is accounted for correctly (see Haser 1995).

The most severe problem of the above procedure is related to the presence of so-called black troughs in saturated profiles, which are extended regions

(corresponding to several hundreds of kilometers per second) in the blue part of the profiles with almost zero residual intensity (cf Figure 1). Without further assumptions, these troughs cannot be fitted because in the usual line formation process, only a very small frequency range (of the order of $v_{\rm th}$) with zero intensity is created. Furthermore, the observed blue absorption edges are much shallower than those resulting from such simple simulations. To overcome both problems, Hamann (1981a,b) introduced a highly supersonic "microturbulence" of the order of Mach 10 present in the entire wind. Because in this case the intrinsic absorption profile becomes much broader, the observed troughs as well as the blue edges can be simulated (for a comprehensive discussion, see Puls 1993). Additionally, the position of the emission peak is redshifted, in agreement with most observations (see also Section 2.4.2). Meanwhile, the assumption of a constant turbulence (used also by Groenewegen & Lamers 1989) has been relaxed (cf Haser 1995) because the justification of a highly supersonic velocity dispersion close to the photosphere is physically problematic, as well as excluded from the non-LTE analysis of photospheric lines in hot stars, resulting in values of $v_{\rm turb}$ below the speed of sound (e.g. Becker & Butler 1992). Thus, in order to fit the profiles, a linear increase of $v_{\rm turb}$ as function of the underlying velocity law is assumed, starting at roughly sonic velocities up to a maximum value $v_{ta}$. The actual values are found in parallel with the determination of $v_\infty$ and $\beta$ from line fits to saturated profile, and typical values for $v_{ta}$ are of the order of $0.1 v_\infty$.

In parallel to the introduction of a velocity dispersion as described above, Lucy (1982a, 1983) suggested an alternative explanation for the black trough generation by means of enhanced backscattering in multiply nonmonotonic velocity fields. Hydrodynamical simulations of time-dependent radiatively driven winds (Owocki et al 1988, Feldmeier 1995) indicate the possibility of such nonmonotonic flows (cf Section 5), and detailed UV line formation calculations on the basis of such models have shown that black troughs are actually created in the profiles of such models (Puls et al 1993a, 1994; Owocki 1994).[1]

### 2.4.2 Optical Lines

Despite the continuous effort to derive mass-loss rates from UV P-Cygni lines, the basic problem remains that one has to know the mean ionization/excitation fractions as well as the element abundances accurately in order to derive reliable numbers. Fortunately, there is an alternative way to determine $\dot{M}$ using the strength of the stellar wind emission in $H_\alpha$ as an indicator of mass-loss rates, where the ionization correction for $H_\alpha$ is much simpler and the hydrogen abundance is usually much less uncertain.

First quantitative non-LTE calculations dealing with the wind emission of hydrogen (and helium lines) go back to Klein & Castor (1978). Then, Leitherer (1988), Drew (1990), Gabler et al (1990), Scuderi et al (1992), and Lamers &

[1]Note that the determinations of $v_\infty$ by Howarth & Prinja (1989) rely in part on the presence of black troughs in saturated CIV lines.

Leitherer (1993) realized the potential of $H_\alpha$ for the determination of mass-loss rates and derived first results for a variety of hot stars. Puls et al (1996) developed a fast method to obtain mass-loss rates from $H_\alpha$ profiles of O-type stars, avoiding some systematic errors inherent in the approach of Leitherer (1988) and Lamers & Leitherer (1993). In the following, we consider some basic issues, including the analysis of $H_\alpha$ from A and late B supergiants. For a comprehensive discussion with a number of detailed profile fits, we refer the reader to Puls et al (1996), McCarthy et al (1997, 1998), Puls et al (1998), and Kudritzki et al (1999).

As pointed out in the introduction to this section, the basic difference of $H_\alpha$ and related lines (including the IR emission lines discussed in the next section) relative to P-Cygni lines concerns the run of the source function, which is rather constant throughout the wind. The latter fact is true as long as those lines are fed predominantly from the spontaneous decay of the upper level or recombinations into both levels, so that the involved occupation numbers are almost in LTE with respect to each other, i.e the source function is almost Planckian. This condition is met for O-stars and early B-stars. For cooler temperatures, however, the feeding of the involved levels from lines of the Lyman series becomes relevant, until in the A-supergiant domain, these lines and the Lyman continuum become optically thick and the corresponding transitions are in detailed balance. Then, the second level of hydrogen (which is the lower one of $H_\alpha$) becomes the effective ground state of HI and the line behaves as a scattering line, thus displaying a typical P-Cygni signature.

***Diagnostic Potential*** Because neutral hydrogen is almost always a trace ion in the winds of OBA stars (excluding the outermost wind and some narrow photospheric recombination region in the A-star domain), the same argumentation as made above for SiIV applies: The opacity of $H_\alpha$ depends on $\rho^2$ (OB-stars) and on $\rho^2/W$ (A-supergiants), so that the actual quantity that can be derived by line fits is $Q^2$, which manifests its sensitivity on and its diagnostic value for the determination of $\dot{M}$. Two instructive examples are given in Figures 2 and 3.

***$H_\alpha$ Emission in O/Early B Stars*** Because of the thermal character of the wind emission and the large emitting volume of the wind, $H_\alpha$ profiles can exhibit enormous equivalent widths and emission peaks, provided the mass-loss rate is large enough. As shown by Puls et al (1996), the equivalent width (absolute value) of the wind emission scales with $Q^{3/2}v_\infty$ for (predominantly) optically thin and with $Q^{4/3}v_\infty$ for optically thick emission. Because of this overlinear dependence on mass loss, the achieved accuracies for $\dot{M}$ (or, more correctly, for $Q$) from lines with large wind emission are enormous and can reach values below 10%. Additionally, because of the strong dependence of opacity on $\rho^2 \propto (r^4v^2)^{-1}$, the shape of the velocity field (i.e. $\beta$) can be determined from the shape of the emission peak. By this method, Puls et al (1996) were able to derive typical values $\beta \approx 1$ for O-type Supergiants, and the results for $Q$ in this domain are in fair agreement with those from the simplified approach used by Leitherer (1988) and Lamers & Leitherer (1993).

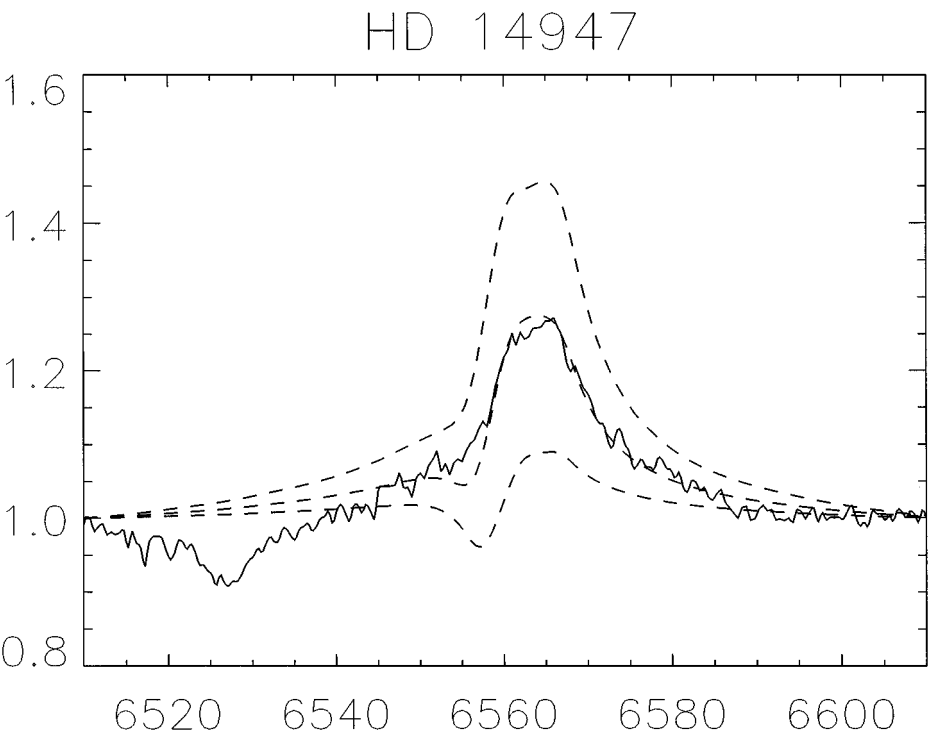


**Figure 2** $H_\alpha$ line profile of the O 5 Ia $f^+$-supergiant HD 14947 compared with line fits as outlined by Puls et al (1996), adopting 10, 7.5, and $5.0 \times 10^{-6}\,M_\odot$/year, respectively, for the mass-loss rate. From Kudritzki (1998).

From the above scaling relations, however, it is also obvious that the emission from thin winds is small and, moreover, almost "hidden" in the normal photospheric profile with a shape dominated by rotational broadening. In these cases, then, detailed calculations on the basis of unified model atmospheres accounting for the transition to photospheric layers (cf Section 2.2) as well as an exact line formation accounting for the finite profile width are required to derive reliable numbers. Without doing this, $Q^2$ is easily overestimated by more than one dex.

In addition to these more theoretical considerations, even with the most elaborate methods, uncertainties up to a factor of 2 in $\dot{M}$ can arise if the absorption profile is only marginally filled and the shape of the velocity field in the lower wind part is not known (e.g. from UV resonance lines): Contrary to the case of strong emission lines, $\beta$ cannot be derived in these cases because the rotationally broadened absorption corrupts all diagnostic clues concerning the wind emission. (The strong dependence of the derived values of $\dot{M}$ on $\beta$ for marginal wind emission can be easily seen from the run of the radial optical depth in the line, $\tau_S \propto Q^2 v(r)^{\frac{1}{\beta}-3}/r^2$.)

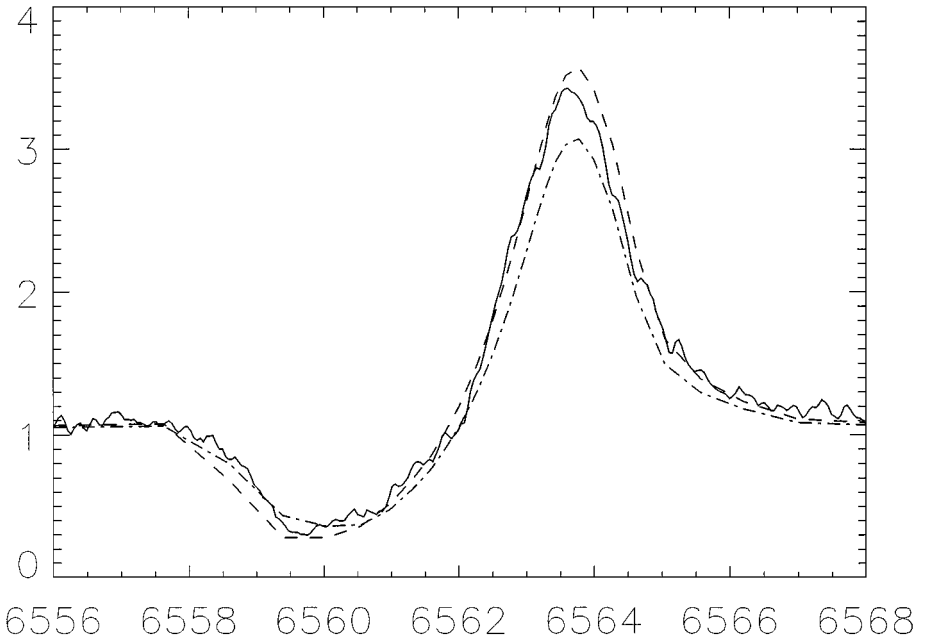


**Figure 3** $H_\alpha$ line profile of the extreme A-supergiant 41-3654 (A3 Ia-O) in the Andromeda Galaxy M31 taken with the Keck HIRES spectrograph compared with two unified model calculations adopting $\beta = 3$, $v_\infty = 200$ km/s and $\dot{M} = 1.7$ and $2.1 \times 10^{-6}$ $M_\odot$/year. Note the P-Cygni profile shape of $H_\alpha$. From McCarthy et al (1997).

***$H_\alpha$ Emission in A/Late B Supergiants*** Because the $H_\alpha$ opacity in the winds of these stars scales with $\rho^2/W$ and the source function is dominated by line scattering, the corresponding profiles are of P-Cygni type and usually visible until up to a frequency corresponding to $v_\infty$, in contrast to the O/B star case, where this is true only for the most luminous objects. The latter fact also allows $v_\infty$ to be derived in parallel with the other quantities and thus enables a complete wind analysis in the optical alone: Because of the additional factor $1/W \approx r^2$, compared with the O-star case from above, and the lower temperature, which increases the ionization fraction of HI significantly, the optical depth in $H_\alpha$ remains large, up to $v_\infty$ in most cases, similar to the behavior of strong UV resonance lines. Analogously, $\beta$ can be derived with significant precision from the profile shape.

A detailed parameter study (based on the unified models by Santolaya-Rey et al 1997) as well as the required fit procedure is given by McCarthy et al (1997, 1998). Kudritzki et al (1999) have used this method to obtain the wind parameters for a large sample of galactic BA-supergiants. In accordance with earlier work by Stahl et al (1991), the derived velocity fields are significantly flatter than for O-stars, with typical values $\beta = 3 \ldots 4$. It is interesting that the observed slope of the blue absorption edges as well as the position of the emission peaks made it

necessary also here to assume the presence of a velocity dispersion, of the order of 10. . . 20 km/s. Note that the terminal velocities of A-type supergiants are a factor of 10 smaller than for O-type stars (cf Section 3).

Of course, the derived values have to be consistent with the observations/simulations of other lines, the most important being the hydrogen Balmer lines. Also, these lines (especially $H_\beta$) are contaminated by wind emission, and only a simultaneous fit of all lines with identical parameters (where $H_\gamma$ provides the required information concerning $\log g$, cf Section 2.3) produces results that can be trusted.



***Problems*** Globally, the errors in $Q$ are of the order of 30%, with smaller values for dense and larger values (the $\beta$ problem) for thin winds. The agreement with mass-loss rates from thermal radio emission (Section 2.4.4) is satisfying (cf Lamers & Leitherer 1993, Puls et al 1996). However, there are also a number of problems, which are illustrated in the following.

In O/early B-stars, the $H_\alpha$ line is contaminated by a blue-ward blend of HeII (separated from the line center of hydrogen by roughly 2 Å corresponding to 100 km/s), which in a number of lines mimics the presence of a P-Cygni type profile, because it is mostly in absorption. In those cases where this blend is strong, present-day simulations are partly unable to fit this component (see Herrero et al 2000). The recipe here is to concentrate on the red wing of the H/He complex, which should give more reliable results because of its weaker contamination by the helium blend, compared with the blue side.

Additionally, a certain variability, which can be severe in the blue absorption troughs of A-star profiles (cf Kaufer et al 1996 and the discussion in Section 5), influences the derived results. Test calculations (see Kudritzki 1999a) have shown that these variations indicate a significant variation for the obtained values of $v_\infty$ and $\dot{M}$ as a function of time. The product of both, i.e. the momentum rate, remains much more constant, however, with a maximum variation of the order of 0.2 dex for the extremely variable wind of HD 92207 (A0Ia).

Another problem results from stellar rotation. The thermal Doppler width of $H_\alpha$ is much smaller than typical rotational velocities of early type stars (of the order of 100 km/s for OB-stars and 30. . . 40 km/s for A-supergiants). Thus, the central emission caused by the wind will certainly be broadened by rotation. Because of conservation of specific angular momentum, the azimuthal velocity in the wind varies according to $v_{\rm rot}(R_*, \theta)/r$, where $v_{\rm rot}(R_*, \theta)$ is the photospheric rotation velocity at co-latitude $\theta$. Thus, for the most important regime of $H_\alpha$ formation ($r = 1 \ldots 1.5$), both the value of $v_{\rm rot}$ itself as well as its variation (i.e., the differential rotation) should have important consequences for the line shape.

Before we further comment on this problem, note that the diagnostics of UV resonance lines in OB-stars are barely affected by this effect, because the stronger lines react only mildly (if at all) to any reasonable value of $v_{\rm rot} \sin i$. In contrast to usual $H_\alpha$ profiles, these resonance lines are formed throughout the wind, which decreases the ratio of $v_{\rm rot} \sin i$ to total line width ($v_\infty$). Moreover, the average

rotational velocities are smaller because $v_{\rm rot} \rightarrow 0$ in the outer wind and the intrinsic Doppler width is larger as a result of the velocity dispersion derived. Note also, however, that rotation might influence the global hydrodynamical structure, a problem we consider in Section 4.2.

With respect to the formation of $H_\alpha$ (and the other Balmer lines, of course), it turns out that the presence of rotation has to be accounted for in order to obtain good fits (except for very strong and very broad emission lines, which, in analogy to strong UV resonance lines, are barely influenced). The usual strategy (cf Puls et al 1996, Herrero et al 2000) is to fold the final profile with a rotational curve of width $v_{\rm rot} \sin i$, where this value can be derived from photospheric metal lines. For a number of (fast rotating) objects, it turns out that the value of $v_{\rm rot} \sin i$ indicated by $H_\alpha$ is smaller than for lines less contaminated by the wind, e.g. $H_\gamma$. This shows clearly the presence of differential rotation in some average sense, in accordance with test calculations by Petrenz & Puls (1996) based on a rigorous treatment of the problem. In conclusion, some average value $\langle v_{\rm rot} \sin i \rangle$ to be determined in parallel with the other parameters becomes an additional part of the $H_\alpha$ fitting procedure, at least for lines that are neither weak ($\langle v_{\rm rot} \sin i \rangle \rightarrow v_{\rm rot} \sin i\,(R_*)$) nor strong.

Of course, the problems discussed here would be of only minor importance if our general assumption of smooth winds (at least in the lower, line-forming region) were severely violated. Because of the intrinsic dependence of the $H_\alpha$ line opacity on $\rho^2$, any significant degree of clumpiness would lead our approach to overestimate the mass-loss rates. We come back to this problem in Section 5.

### 2.4.3 IR Lines

The dramatic progress of IR astronomy in the past decade has opened a completely new window for the systematic investigation of winds around hot stars. In their first paper on unified model atmospheres, Gabler et al (1989) realized the importance of IR emission and absorption lines for a quantitative understanding of the physics of hot star atmospheres and winds and pointed out the potential of this new spectral range. A wealth of observational material is now available (see, for instance, Hanson et al 1996, Figer et al 1997) for quantitative work.

The theoretical framework for the analysis of IR spectra is in principle identical to that of the optical and UV lines. As for those cases, the IR spectra of hot stars also show pure emission lines, P-Cygni profiles, and wind-contaminated absorption lines. However, because the IR continuum of objects with strong winds (contrary to the optical continuum) is formed in the supersonic part of the wind, IR lines sample different depths of a stellar wind and give additional information about the shape of the velocity field. Najarro et al (1997a), Lamers et al (1996), and Hillier et al (1998) have investigated this important effect using high-quality ground-based (optical and IR) and ISO IR spectra.

The winds of hot stars of extreme luminosity and with strong IR emission characteristics in the galactic center have been investigated by Najarro et al (1994, 1997b) and Figer et al (1998). Crowther et al (1998) have provided beautiful

diagnostics of late Of-supergiants and WNL stars in order to probe wind-velocity fields, effective temperatures, and blanketing effects in the photospheric EUV continua.

In the case of very thin winds with extremely low mass-loss rates, IR line profiles turn out to be outstanding diagnostic tools for the determination of mass-loss rates, clearly superior to optical lines such as $H_\alpha$. Because $h\nu/kT \ll 1$ in the IR, stimulated emission becomes important, and non-LTE effects in the line (caused by the presence of the wind) are substantially amplified (Mihalas 1978, Kudritzki 1979), leading to strong emission even for very small mass-loss rates, as has been pointed out by Najarro et al (1998).



### 2.4.4 IR, Submillimeter, and Radio Continua

Not only the spectral lines but also the IR, (sub)millimeter, and radio continua can be used to analyze the properties of the wind plasma. Actually, they constitute one of the most reliable diagnostic tools for this purpose because they are based on simple atomic/radiation transfer processes, whereas lines usually require consideration of a number of nasty details, such as non-LTE, line broadening, etc.

The basic idea is to investigate the excess relative to the flux predicted by photospheric model atmospheres, which is attributed to free-free ("Bremsstrahlung") and bound-free emission in the winds, and which because of the $\lambda^3$ dependence of the corresponding opacities and the resulting geometrical increase of the effective photosphere becomes significant at longer wavelengths. In most cases, the emission arises from thermal electrons (deduced from the spectral index of the radiation, see below); however, there exists also a significant fraction (roughly 30%) of nonthermal emitters (Bieging et al 1989 and references therein; see also Altenhoff et al 1994). In the following, we mainly discuss thermal emission; we briefly consider nonthermal effects at the end of this subsection (see also Section 5).

The pioneering work on IR and radio free-free emission from hot star winds was presented independently by Wright & Barlow (1975) and Panagia & Felli (1975). Both publications showed that the continuum flux $S_\nu$ at long wavelengths for an optically thick, spherically symmetric and isothermal envelope expanding at constant velocity scales with $S_\nu \propto \nu^{0.6}$. Moreover, the observed radiation depends only weakly on the electron temperature in the wind and is set essentially by the distance to the star $d$, the mass-loss rate, and the terminal velocity via

$$S_\nu \propto \left(\frac{\dot{M}}{v_\infty}\right)^{4/3} \frac{\nu^{0.6}}{d^2}, \qquad (7)$$

where we have suppressed additional dependences on the chemical composition, ionization stage, and Gaunt-factors. (For effects of different density and temperature stratifications, see Cassinelli & Hartmann 1977, Bertout et al 1985.)

The exclusive use of radio observations, however, is problematic. Because the excess flux (i.e. total flux in the radio domain) scales with $\nu^{0.6}$, OB-stars will be generally weak radio sources (which prohibits the use of this method for

extragalactic work), and useful radio observations can be obtained only for nearby stars with dense winds. Moreover, because the spectral index of a nonthermal component is negative (e.g. $-0.7$ for synchrotron emission), the radio domain can be more easily contaminated than shorter wavelengths, e.g. the (sub)millimeter regime (see Altenhoff et al 1994, Contreras et al 1996).

By concentrating on lower frequencies, however, at least in the IR, the presence of a velocity stratification has to be accounted for, as was pointed out by Wright & Barlow (1975): In contrast to the radio/submillimeter regime, the wind becomes optically thick at velocities well below $v_\infty$. By using a velocity law with a shape that fitted the IR continuum of P-Cygni, Barlow & Cohen (1977) took these problems into account and performed an extensive IR analysis of some 40 OBA supergiants.

The effects of a more general velocity field, together with the inclusion of bound-free opacities and an estimate concerning the influence of electron scattering (important only at very high wind densities, e.g. in the winds of Wolf-Rayets), were discussed by Lamers & Waters (1984a). They expressed the nondimensional excess in terms of a curve of growth, from which the velocity law and the mass-loss rate can be derived simultaneously. Extensive tables of curves of growth as well as the required gaunt factors as functions of chemical composition were published by Waters & Lamers (1984).

***Mass-Loss Rates from Radio/Submillimeter Observations*** Early radio measurements (mostly with the VLA at 2 and 6 cm) and subsequent determinations of mass-loss rates of O/early B-star winds have been published by Abbott et al (1980, 1981) and Bieging et al (1989). For a number of these stars, Howarth & Brown (1991) have added VLA fluxes at 3.6 cm. These measurements (see also the catalogue compiled by Wendker 1987) provide one of the most complete data sets and have been used, for example, in the comparison with $H_\alpha$ mass-loss rates by Lamers & Leitherer (1993) and Puls et al (1996), as well as for the calibration of "empirical ionization" fractions (Lamers et al 1999a) (see Section 2.4.1). Recently, Leitherer et al (1995) studied a number of (very) dense winds (including two Of-star winds) with the Australia telescope compact area at 3.5 and 6.25 cm, and Scuderi et al (1998) have detected another seven new OB radio sources with the VLA. Radio observations of later spectral types (supergiants between B2 and F8) have been performed by Drake & Linsky (1989) and were used by Kudritzki et al (1999) to compare with corresponding $H_\alpha$ data. Because most of these observations comprise at least two frequency points, and taking into account the 1.3-mm observations by Leitherer & Robert (1991) performed with the Swedish-ESO submillimeter telescope at La Silla, the presence of nonthermal components could be easily detected from the spectral index. Of course, only those objects with purely thermal emission have been used to derive mass-loss rates. In addition to the data by Leitherer & Robert, Altenhoff et al (1994) have observed approximately 20 OB stars at 1.2 mm with the IRAM 30-m telescope at Pico Veleta.

Because of the enormous extension of the radio photosphere for objects with large $\dot{M}$, it is, in principle, also possible to resolve the radio-emitting region.

In this way, White & Becker (1982; see also Skinner et al 1998) resolved the wind of P-Cygni at 6 cm and found an apparently spherically symmetric wind at an electron temperature of 18,000 $\pm$ 2,000 K, i.e., of the order of $T_{\rm eff} \approx 18,500$ K.

***IR Excess*** Following the work by Barlow & Cohen (1977), who found significant excess for a number of objects at 10 $\mu$ (for some objects down to 2.2 $\mu$), Tanzi et al (1981), Castor & Simon (1983), and Abbott et al (1984b) tried to derive $\dot{M}$ (and partly the shape of the velocity fields) for a number of OB stars from the IR excess in various bands. Bertout et al (1985) analyzed a large sample of early-type stars in OB associations and pointed out that reliable measurements of the excess are only possible for stars with significant wind density ($\dot{M} \geq 10^{-6}\,{\rm M}_\odot/{\rm a}$) and/or a flat velocity profile. IRAS observations between 10 ... 100 $\mu$ were used to analyze one of the Rosetta-stones among stellar winds, the wind of $\zeta$ Pup (O4 If). From these observations, Lamers et al (1984) could exclude older models, claiming a hot or warm base corona (thus again, wind temperature $\approx T_{\rm eff}$), and derived a mass-loss rate and velocity profile with $\beta = 1$, in agreement with current findings from $H_\alpha$. A recent reanalysis of most of the described data (IR excess and radio fluxes simultaneously) was performed by Runacres & Blomme (1996), who found that the majority of the observations are consistent with current theoretical work. For four of their program stars (including $\zeta$ Pup and $\alpha$ Cam), however, they claimed the presence of an additional emission mechanism.[2]

***Problems*** Generally, the agreement between the radio and IR diagnostics on the one side and the $H_\alpha$ analysis on the other is satisfying (cf Lamers & Leitherer 1993, Puls et al 1996, Kudritzki et al 1999). However, there are also problematic cases (see above) connected with too high an IR excess compared with radio and $H_\alpha$ measurements. An instructive example is discussed by Kudritzki et al (1999) for the case of HD 53138 (B3Ia), where the $H_\alpha$ measurement is consistent with the (upper limit) of the observed radio flux from Drake & Linsky (1989). In contrast, the 10-$\mu$ excess derived by Barlow & Cohen (1977), which is also peculiarly high compared with other wavelengths, would result in $\dot{M}$ a factor 20 higher. By investigating the data published in the CDS Catalog of Infrared Observations, Gezari et al (1999) discovered that many stars show a significant scatter in the IR photometry, which might be attributed to a photometric variability of B-supergiants. Thus, the "measurement" of an IR excess (requiring the "subtraction" of combined wind plus photospheric fluxes in the IR and purely photospheric fluxes in the optical/near IR) becomes difficult unless the complete energy distribution is observed simultaneously.

An alternative explanation might be given by the presence of clumping, which, in analogy to the case of $H_\alpha$, would increase the IR excess due the $\rho^2$-dependence

[2] Investigations by F Najarro (private communications) have shown that consistent solutions can be obtained also in those cases with a $\beta$-value larger and a mass-loss rate smaller than those derived from $H_\alpha$.

of opacity. (The inconsistency of IR and $H_\alpha$ fluxes would then point to depth-dependent clumping factors; cf Section 5). Simple methods to incorporate clumping in the IR diagnostics have been proposed by Abbott et al (1981) and Lamers & Waters (1984b). A first comparison with time-dependent models has been given by Puls et al (1993b), and on the basis of a simplified "partial shell" description, Blomme & Runacres (1997) have pointed out that a small amount of clumping is sufficient to reconcile the discrepancies found in their previous work.

***Nonthermal Emission*** As mentioned earlier, there is ample evidence of nonthermal emission in hot star winds. First observational findings were reported by White & Becker (1983) and Abbott et al (1984a), and latest measurements (for WRs) were presented by Chapman et al (1999). Although it seems clear that the nonthermal emission is due synchrotron radiation from relativistic electrons, different agents responsible for the acceleration are discussed in the literature: wind accretion onto compact objects (Abbott et al 1984a), wind-wind collisions in binary systems (Stevens 1995), magnetic reconnection in single or colliding winds (Pollock 1989), and first-order Fermi acceleration in the shocks (randomly) distributed in stellar winds (Chen & White 1994), which are thought to be responsible for the emission of X-rays as well (discussed in the following).

### 2.4.5 X-Ray Emission

Among the first surprising discoveries of the Einstein observatory was the detection that all O-stars are soft X-ray emitters (Harnden et al 1979, Seward et al 1979). It was soon found that the X-ray luminosity is roughly correlated with the stellar luminosity: $\log L_x/L_{\rm bol} \approx -7 \pm 1$ (Seward et al 1979, Pallavicini et al 1981, Chlebowski et al 1989). The scatter in this relation is very large, indicating a dependence on additional parameters.

The source of the O-star X-ray emission is widely believed to be shocks propagating through the stellar wind (Lucy & White 1980, Lucy 1982b, Cassinelli & Swank 1983, MacFarlane & Cassinelli 1989), where the shocks may result from a strong hydrodynamic instability of radiation-driven winds (see also Section 5). ROSAT and ASCA observations of O- and B-stars have confirmed this interpretation (Hillier et al 1993; Cassinelli et al 1994; Cohen et al 1996, 1997a,b; Berghöfer et al 1997). Assuming a simple model of randomly distributed shocks in a stellar wind, where the hot shocked gas is collisionally ionized and excited and emits spontaneously into and through an ambient "cool" stellar wind with a kinetic temperature of the order of the effective temperature, these authors were able to determine shock temperatures, filling factors, and emission measures. The diagnostic situation differs between B-stars, where the winds are usually optically thin at X-ray wavelengths, and O-stars, where the winds can become optically thick and X-ray radiative transfer is needed. For the latter case, Feldmeier et al (1997a) have developed a refined diagnostic model, including postshock cooling zones for radiative and adiabatic shocks. Kudritzki et al (1996) applied these techniques on a larger sample of O-stars observed with ROSAT and found a dependence of

the filling factor of the X-ray emission on $\bar{\rho}$ (which is proportional to the inverse cooling length of the shocks), leading to an additional dependence of $\log L_x$ on the average density in the stellar wind. By a simple scaling analysis of the involved X-ray emission and absorption processes, Owocki & Cohen (1999) showed that the "natural" scaling for optically thin winds is given by $L_x \propto (\dot{M}/v_\infty)^2$ and for optically thick winds by $L_x \propto (\dot{M}/v_\infty)^{1+s}$, if one assumes a radial dependence of the filling factor as $f \propto r^s$. The loose correlation $L_x \propto L_{\rm bol}$ for thick winds can then be reproduced, if one allows for a modest radial falloff of this quantity ($s \approx -0.25 \ldots -0.4$).

An alternative model has been suggested by Feldmeier et al (1997b) based on detailed time-dependent hydrodynamic models, where cloud collisions in an inhomogeneous wind lead to X-ray emission.

For the analysis of stellar winds, the existence of X-ray emission is important for two reasons. First, their direct spectral diagnostics—particularly in view of the X-ray telescope with spectrographs of sufficient resolving power, such as the Chandra satellite—will allow investigation of the limitations of the standard model, discussed in Section 2.1. Here a particularly promising approach is the simultaneous investigation of optical line and X-ray variability (Berghöfer et al 1996, Berghöfer & Schmitt 1994). Second, the X-rays and EUV photons emitted by the shocks severely affect the degree of ionization of highly ionized species, such as CIV, NV, and OVI and the diagnostics of their resonance lines observable in the far UV (see MacFarlane et al 1993, Pauldrach et al 1994, Taresch et al 1997, Haser et al 1998). In this sense, they introduce an additional uncertainty as long as the modeling of the shock emission is not constrained well enough.



## 3. RESULTS

The diagnostic methods of stellar winds described in the previous section have been applied to a large number of early-type stars. In this section, we discuss the results of these studies, in particular the empirical correlations of the global stellar wind parameters with stellar parameters. We first discuss terminal velocities, mass-loss rates, and wind momenta of galactic stars and then we investigate the influence of stellar metallicity by a comparison with stars in the Magellanic clouds.

### 3.1 Terminal Velocities of Winds from Galactic Hot Stars

In two pioneering papers compiling terminal velocities of winds from massive hot stars as a function of stellar parameters, Abbott (1978, 1982) demonstrated for the first time the existence of a correlation with effective temperature and photospheric escape velocity. These papers have induced a number of systematic and comprehensive studies using refined diagnostic methods and analyzing the full UV spectroscopic material available from IUE and HST high (and medium) resolution observations. We mention here the work by Groenewegen et al (1989),

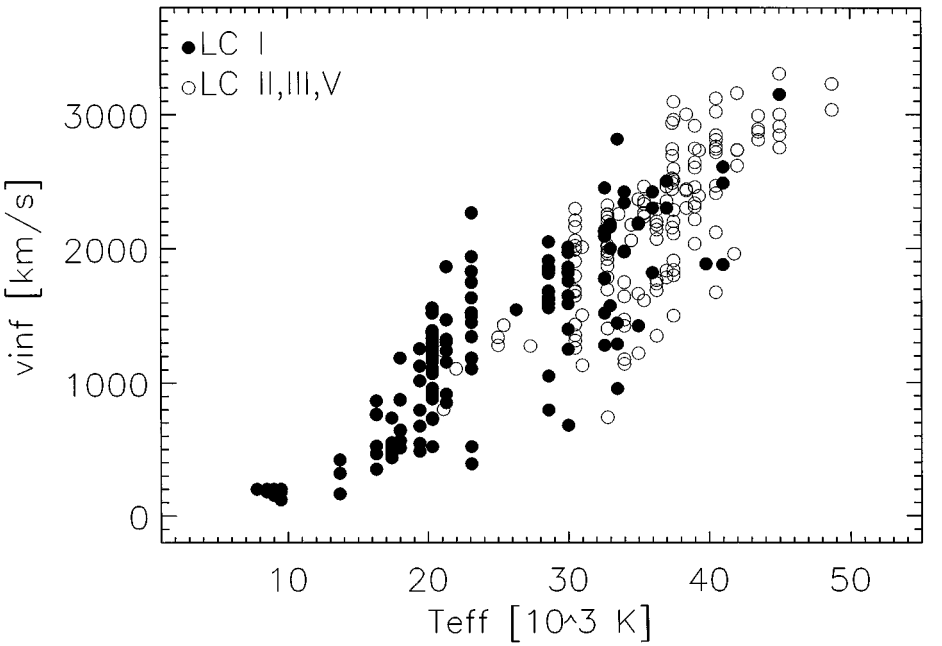


**Figure 4** Terminal velocities as a function of effective temperature for massive hot stars of different luminosity classes. The data for B- and O-stars ($T_{\rm eff} \geq 10{,}000$ K) are taken from Prinja et al (1990), Prinja & Massa (1998), and Howarth et al (1997), who used the effective temperature scale of Humpreys & McElroy (1984) for the conversion of spectral type to $T_{\rm eff}$. The data for A-supergiants ($T_{\rm eff} \leq 10{,}000$ K) are from Lamers et al (1995).

Groenewegen & Lamers (1989), Howarth & Prinja (1989), Prinja et al (1990), Lamers et al (1995), Haser (1995), and Howarth et al (1997) on massive stars in the Galaxy. These papers have convincingly confirmed the correlations proposed by Abbott and have provided quantitative coefficients to describe them on a solid statistical basis.

Figure 4 demonstrates that $v_\infty$ and spectral type or $T_{\rm eff}$, respectively, are correlated. Table 1 gives average values as a function of spectral type. Because terminal velocities can usually be measured with an accuracy of 10% (see the previous section) and the determination of spectral type is usually accurate to one subclass, the scatter must have an intrinsic physical reason. We attribute it to the fact that the dependence of $v_\infty$ on $T_{\rm eff}$ is indirect through the photospheric escape velocity $v_{\rm esc}$, which becomes smaller with smaller $T_{\rm eff}$ for main sequence stars and when massive stars evolve toward lower temperatures to become supergiants. This means that, on the average, stars with lower effective temperature are expected to have slower winds. However, at a given effective temperature, even stars of similar luminosity class will have different gravities and different photospheric escape velocities, leading to a significant spread of terminal velocities.

**TABLE 1** Terminal velocities of massive hot stars: O-stars and B- and A-supergiants[a]

| Sp. type | LC I | LC II | LC III | LC V | Sp. type | LC Ia | LC Ib |
|---|---|---|---|---|---|---|---|
| O3 | 3000 | | | 3200 | B0 | 1450 | 1700 |
| O4 | 2400 | | | 3000 | B0.5 | 1450 | 1400 |
| O5 | 2100 | | 2800 | 2900 | B1 | 1200 | 1000 |
| O5.5 | 2000 | | | | B1.5 | 780 | 950 |
| O6 | 2300 | | 2500 | 2600 | B2 | 540 | 840 |
| O6.5 | 2200 | | 2600 | 2600 | B3 | 490 | |
| O7 | 2100 | 2400 | 2600 | 2400 | B5 | 270 | 470 |
| O7.5 | 1900 | 2300 | 2300 | 2100 | A0 | 160 | 180 |
| O8 | 1500 | 2000 | 2200 | 1900 | A1 | 160 | |
| O8.5 | 2000 | | 2300 | 1900 | A2 | 170 | |
| O9 | 1900 | 2100 | 2000 | 1500 | A3 | 180 | |
| O9.5 | 1700 | 1720 | 1600 | | A5 | 180 | 180 |
| O9.7 | 1700 | 2000 | | | A8 | | 200 |

[a]Data for O-supergiants from Prinja et al (1900) and Haser (1995); data for B-supergiants from Prinja & Massa (1998); data for A-supergiants from Lamers et al (1995).



The direct dependence on the photospheric escape velocity is shown in Figure 5, again as a function of $T_{\rm eff}$. It is important to note that the photospheric escape velocity includes the reducing effect of Thomson scattering on the gravitational potential

$$v_{\rm esc} = (2g_* R_* (1 - \Gamma))^{0.5}, \tag{8}$$

where $g_*$ is the photospheric gravity and $\Gamma$ the ratio of radiative Thomson to gravitational acceleration.

From the definition of $v_{\rm esc}$, it is clear that the determination of stellar escape velocities requires the knowledge of stellar masses and radii. For the construction of Figure 5, this has been done by adopting effective temperature, bolometric correction, and absolute magnitude calibrations as a function of spectral type and luminosity class to determine stellar luminosities, which are then used to estimate stellar masses from evolutionary tracks. In Section 2.3 we mentioned the "mass discrepancy" between masses determined in this way and masses determined from individual NLTE spectral analyses of objects with well-known distances, which yield individual effective temperatures, gravities, and radii with presumably higher precision. Figure 6 compares results obtained by these two alternative methods in the case of supergiants of luminosity class I, where the effects of the "mass discrepancy" is expected to be largest. There are indications of small systematic effects, but the general result is similar. For effective temperatures larger than 21,000 K, the ratio of $v_\infty$ to $v_{\rm esc}$ appears to be roughly constant. At 21,000 K, there is a sudden

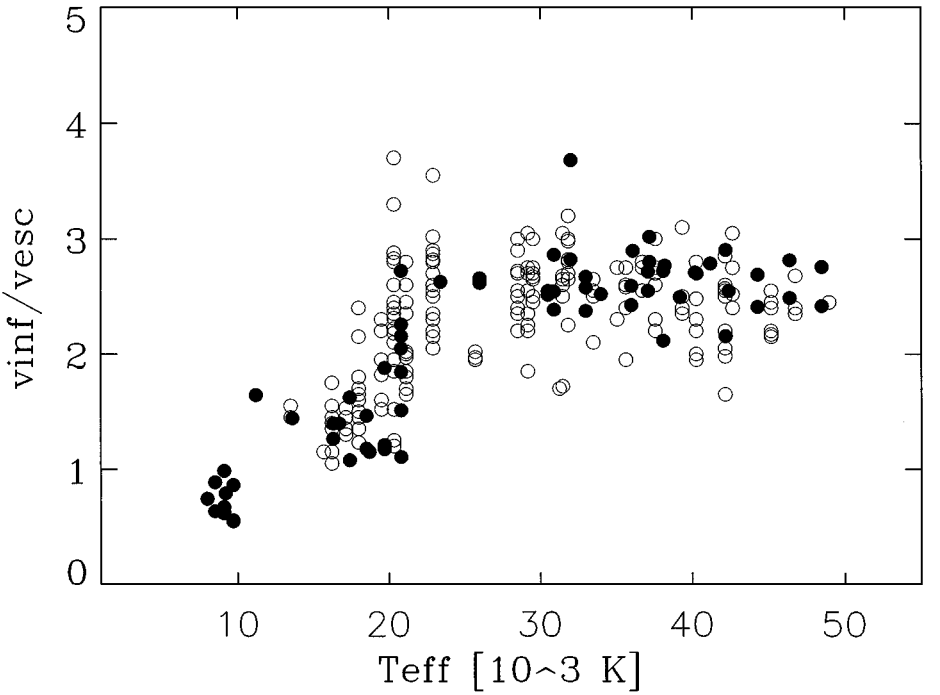


**Figure 5** The ratio of terminal velocity to photospheric escape velocity as a function of effective temperature. (*Open symbols*) Prinja & Massa (1998); (*solid symbols*) Lamers et al (1995).



transition toward a significantly smaller but also constant ratio (Lamers et al 1995), which is interpreted as the result of the fact that because of changes in ionization, different ionic species start to drive the wind (for further discussion and references see Section 4). Another step in the $v_\infty$ to $v_{\rm esc}$ ratio might be present at 10,000 K, although the few results from the individual spectroscopic analyses in this temperature range obtained by Kudritzki et al (1999) do not fully confirm such a conclusion. Summarizing the results from Howarth & Prinja (1989), Prinja et al (1990), Lamers et al (1995), Howarth et al (1997), Prinja & Massa (1998), Puls et al (1996), and Kudritzki et al (1999), a reasonable scaling formula for the terminal velocity is given by

$$v_\infty = C(T_{\rm eff})\, v_{\rm esc}, \qquad \begin{cases} C(T_{\rm eff}) = 2.65, & T_{\rm eff} \geq 21{,}000\,{\rm K} \\ C(T_{\rm eff}) = 1.4, & 10{,}000\,{\rm K} < T_{\rm eff} < 21{,}000\,{\rm K} \\ C(T_{\rm eff}) = 1.0, & T_{\rm eff} \leq 10{,}000\,{\rm K}. \end{cases} \quad (9)$$

The accuracy of $C(T_{\rm eff})$ is roughly 20%.

A completely independent confirmation of the correlation of terminal with photospheric escape velocities comes from the investigation of Central Stars of

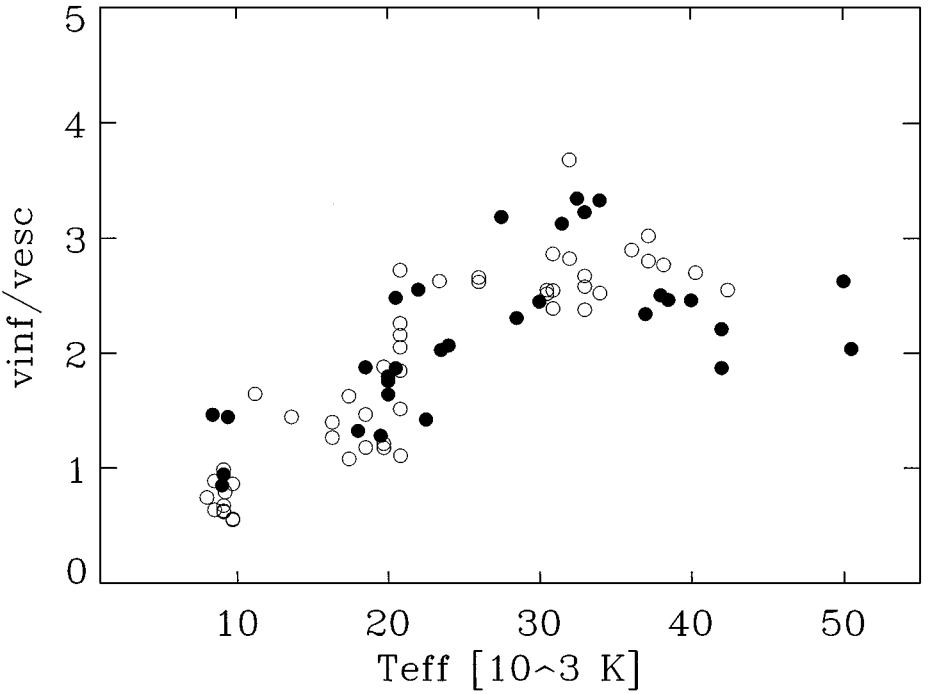


**Figure 6** The ratio of terminal velocity to photospheric escape velocity as a function of effective temperature for supergiants of luminosity class I. (*Open symbols*) Lamers et al (1995); (*solid symbols*) Puls et al (1996), Kudritzki et al (1999). Note that for the *solid symbols*, the escape velocities are obtained from detailed non-LTE analyses of individual objects.



Planetary Nebulae (CSPN). Although these objects have a completely different stellar interior and are in a completely different phase of stellar evolution, as post-AGB objects of 0.5–0.7 $M_\odot$, they are certainly (very) hot stars. They evolve from the AGB toward very hot temperatures with roughly constant luminosity. Many of them have optical and UV spectra similar to O-stars. Spectroscopic non-LTE studies carried out by Méndez et al (1988), Perinotto (1993), and Kudritzki et al (1997) and using the same diagnostic techniques as outlined in Section 2 have made it possible to constrain the evolution of these objects and to estimate stellar distances and masses. They have also allowed a discussion of stellar wind properties along the evolution, with constant luminosity and constant mass from the right to the left in the HRD (see also Pauldrach et al 1989).

Figure 7 shows the striking relationship of $v_\infty$ with $T_{\rm eff}$ for these objects. The interpretation of this diagram is straightforward. Because CSPN shrink during their evolution toward higher temperatures, their photospheric escape velocity increases, and the terminal velocity, which depends on $v_{\rm esc}$, increases as well. Adopting an average mass of 0.58 $M_\odot$ for these post-AGB objects (comparable to

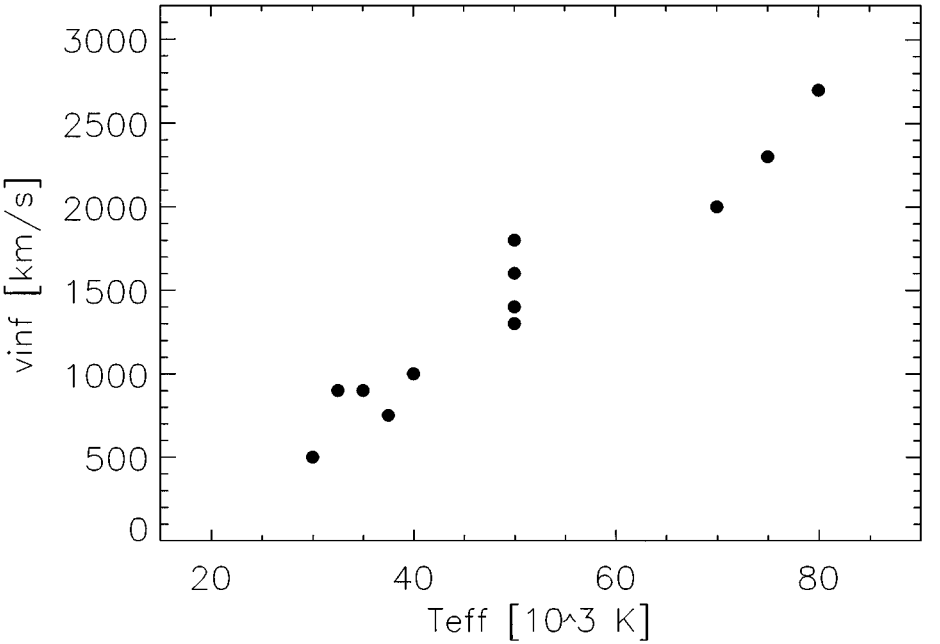


**Figure 7** Terminal velocities of winds from Central Stars of Planetary Nebulae with O-type spectra as a function of effective temperature. Data are from Méndez et al (1988), Pauldrach et al (1989), Perinotto (1993), Haser (1995), and Kudritzki et al (1997).



the average mass of white dwarfs) (see Napiwotzki et al 1999) and a corresponding luminosity according to the core mass–luminosity relationship (see Schönberner 1983, Wood & Faulkner 1986), one can calculate escape velocities for each object of Figure 7 and compare the ratio of $v_\infty$ to $v_{\rm esc}$ with the case of O-stars. In this way, agreement with the O-stars at least for CSPN with $T_{\rm eff} \leq 50{,}000$ K is obtained. However, as stressed by Kudritzki et al (1997), much smaller escape velocities and ratios $v_\infty$ to $v_{\rm esc}$ of the order of 3–5 are found if gravities and radii from their non-LTE spectroscopy are used directly. Kudritzki et al (1997) attribute this disagreement to either some unknown defect of their spectral analysis procedure or a failure of the core mass–luminosity relationship applied.

## 3.2 Mass-Loss Rates and Wind Momenta of Galactic Hot Stars

During the past 3 years there have been comprehensive studies to reinvestigate the mass-loss rates of galactic hot stars by analyzing $H_\alpha$ profiles based on unified non-LTE model atmospheres. Because the only requirement is that a good spectrum can be taken, this method can determine mass-loss rates for a much larger number of objects than the method analyzing radio emission.

Puls et al (1996) and Herrero et al (2000) have investigated the mass-loss rates of O-stars. Kudritzki et al (1997) studied CSPN, and Kudritzki et al (1999) determined mass-loss rates of galactic A- and B-supergiants. In the following, we summarize their results.

The best way to discuss the strengths of stellar winds is in terms of the wind momentum–luminosity relationship (WLR). Because the winds of hot stars are driven by radiation, it is intuitively clear that the mechanical momentum of the stellar wind flow should be mostly a function of photon momentum. Indeed, the theory of radiation-driven winds predicts (see discussion in Section 4) that the "modified stellar wind momentum" depends directly on luminosity through the WLR

$$\log D_{\rm mom} = \log D_0 + x \log(L/L_\odot), \qquad D_{\rm mom} = \dot{M} v_\infty (R_*/R_\odot)^{0.5}. \qquad (10)$$

The coefficients of the WLR, $\log D_0$ and $x$, are expected to vary as a function of spectral type and luminosity class.

Figure 8 shows modified wind momenta of O-stars and CSPN as a function of luminosity. It is obvious that the O-supergiants follow a tight WLR, as described by Equation 10 over at least 1 dex in luminosity. The coefficients of the corresponding

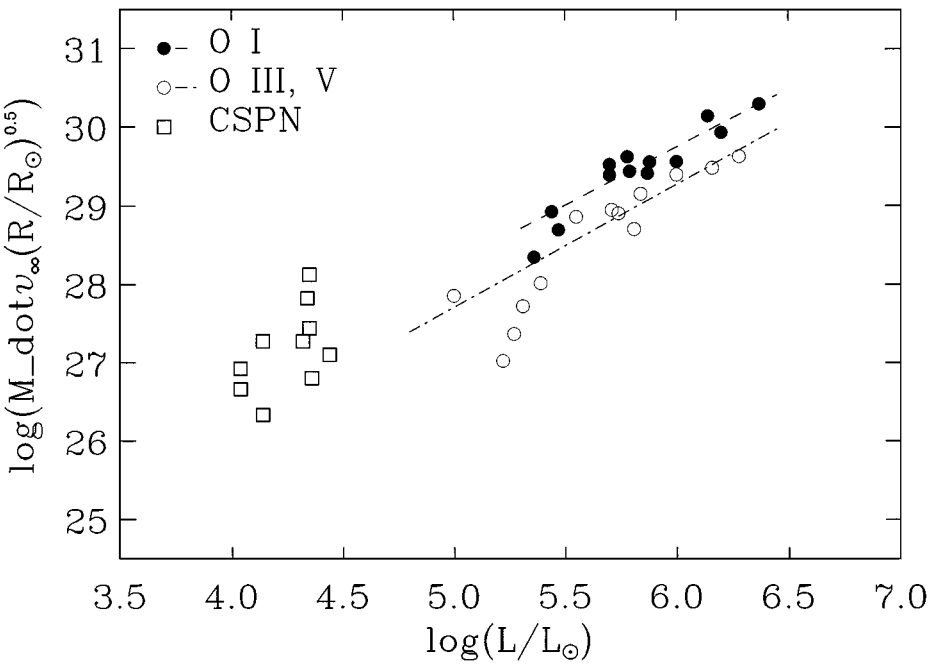


**Figure 8** Modified wind momenta of galactic O-stars and Central Stars of Planetary Nebulae (CSPN) as a function of luminosity. The wind momentum–luminosity relationship for O-supergiants and O-giants/dwarfs obtained by linear regression are also shown. Data from Puls et al (1996), Herrero et al (1999b), and Kudritzki et al (1997).

**TABLE 2** Coefficients of the wind momentum–luminosity relationship for A/B-supergiants and O-stars of the solar neighborhood

| Sp. type | Log $D_0$ | x | $\alpha'$ |
|---|---|---|---|
| A I | 14.22 ± 2.41 | 2.64 ± 0.47 | 0.38 ± 0.07 |
| Mid B I | 17.07 ± 1.05 | 1.95 ± 0.20 | 0.51 ± 0.05 |
| Early B I | 21.24 ± 1.38 | 1.34 ± 0.25 | 0.75 ± 0.15 |
| O I | 20.69 ± 1.04 | 1.51 ± 0.18 | 0.66 ± 0.06 |
| O III, V | 19.87 ± 1.21 | 1.57 ± 0.21 | 0.64 ± 0.06 |



linear fit are given in Table 2. The situation for O-giants and -dwarfs is similar; however, the WLR is shifted downward to lower wind momenta, and at the low luminosity end the situation is somewhat confusing. Two objects ($\zeta$ Oph and HD 13268) with $\log L/L_\odot \leq 5.3$ fall clearly below the relationship. Both are rapid rotators with very thin winds. Several additional effects may become important in such a situation, as is discussed in Section 4.

The fact that the CSPN as objects of significantly lower luminosity and of completely different evolutionary status have wind momenta corresponding to the extrapolation of the WLR of O-stars must be regarded as an encouraging success of the interpretation of winds in terms of radiative driving and of the concept of the WLR.

Figure 9 compares wind momenta of O-, B-, and A-supergiants. For all these different spectral types, a tight relationship between wind momentum and luminosity is found. However, the WLR varies as a function of spectral type. Wind momenta are strongest for O-supergiants, then decrease from early B (B0 and B1) to mid B (B1.5 to B3) spectral types and become stronger again for A-supergiants. The slope of the WLR appears to be steeper for A- and mid B-supergiants than for O-supergiants. The interpertation of this result is given in Section 4.

## 3.3 Observed Effects of Metallicity: The Magellanic Clouds

It is obvious that the global properties of winds must depend on metallicity. Because the winds of hot stars are driven by photon momentum transfer through metal line absorption, certainly the wind momentum rate and possibly the terminal velocities must be a function of stellar metallicity. The ideal laboratory to test the metallicity dependence are the Magellanic clouds.

Figure 10 compares terminal velocities of O-stars in the Galaxy, the large Magellanic cloud (LMC), and the small Magellanic cloud (SMC). Although there is a large scatter in this diagram, because stars of different luminosity classes and photospheric escape velocities are not disentangled, there is a clear indication that, on the average, wind velocities in the metal-poor SMC are smaller. For the LMC, the situation is not so clear.

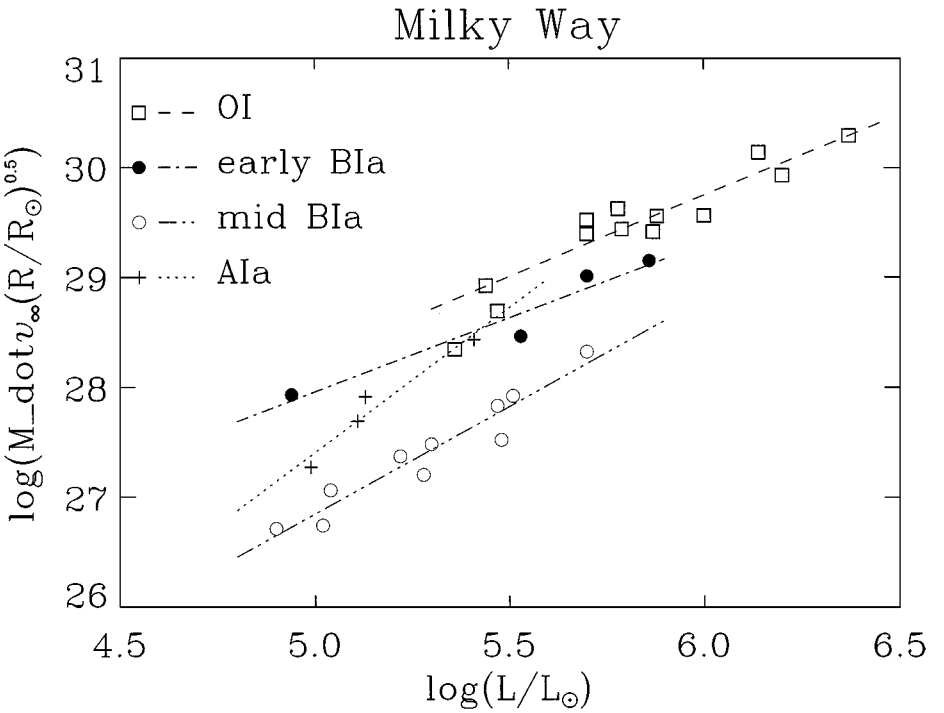


**Figure 9** Wind momenta of galactic O-, early B-, mid B-, and A-supergiants as a function of luminosity together with the corresponding wind momentum–luminosity relationship obtained by linear regression. Data from Puls et al (1996), Herrero et al (1999b), and Kudritzki et al (1999).

Wind momenta of O-stars show a definite trend with metallicity. This is demonstrated by Figure 11. Although the number of objects studied in the clouds is still small, it is clear that average momenta in the LMC are smaller than in the Galaxy and average momenta in the SMC are smaller than in the LMC. Puls et al (1996) quote a difference of 0.20 and 0.65 dex between the Galaxy and the LMC or SMC, respectively.

In their study of very massive stars in the compact cluster R136a in the LMC, de Koter et al (1998) find very high wind momenta for their most luminous objects, indicating a much steeper WLR than that found by Puls et al (1996). This discrepancy is to a large extent the result of the different effective temperature determinations used. de Koter et al use the OV $\lambda$ 1371 line as a temperature indicator based on their model atmosphere calculations, whereas Puls et al used the optical HeI $\lambda$ 4471 line. It is not clear which of the two methods is closer to the truth. Careful future spectroscopic work based on fully consistent hydrodynamic line-blanketed non-LTE models is needed to clarify the situation.

Large observing programs of A- and B-supergiants in the Magellanic clouds are currently under way to investigate the influence of metallicity at later spectral

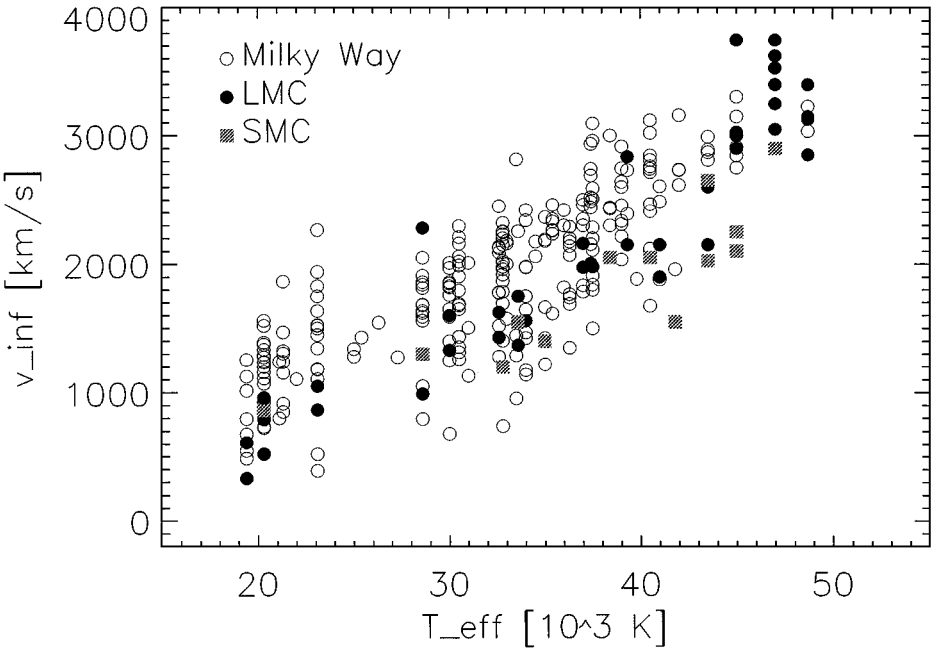


**Figure 10** Terminal velocities of O-stars in the Galaxy, large Magellanic cloud (LMC), and small Magellanic cloud (SMC) as a function of effective temperature. For the conversion of spectral type into effective temperature, the scale by Humphreys & McElroy (1984) was used for simplicity. Data from Howarth et al (1997), Prinja & Crowther (1998), de Koter et al (1998), Puls et al (1996), and Haser (1995).

types. In addition, a large number of O-stars have been observed very recently in both clouds with HST. These programs will allow determination of the role of metallicity much more precisely.

## 4. INTERPRETATION BASED ON THE THEORY OF LINE-DRIVEN WINDS

As mentioned in the previous sections, the basic mechanism driving the winds of hot stars is the transfer of photospheric photon momentum to the stellar atmosphere plasma through absorption by spectral lines. Obviously, the properties of stellar winds must depend on the number of lines being available to absorb significant amounts of photon momentum, in particular at wavelengths around the photospheric flux maximum. However, not only is the number of lines important; their ability to absorb, i.e. their optical thickness, is also important. In supersonically expanding winds, optical thickness is a local quantity, as described by Equations 4

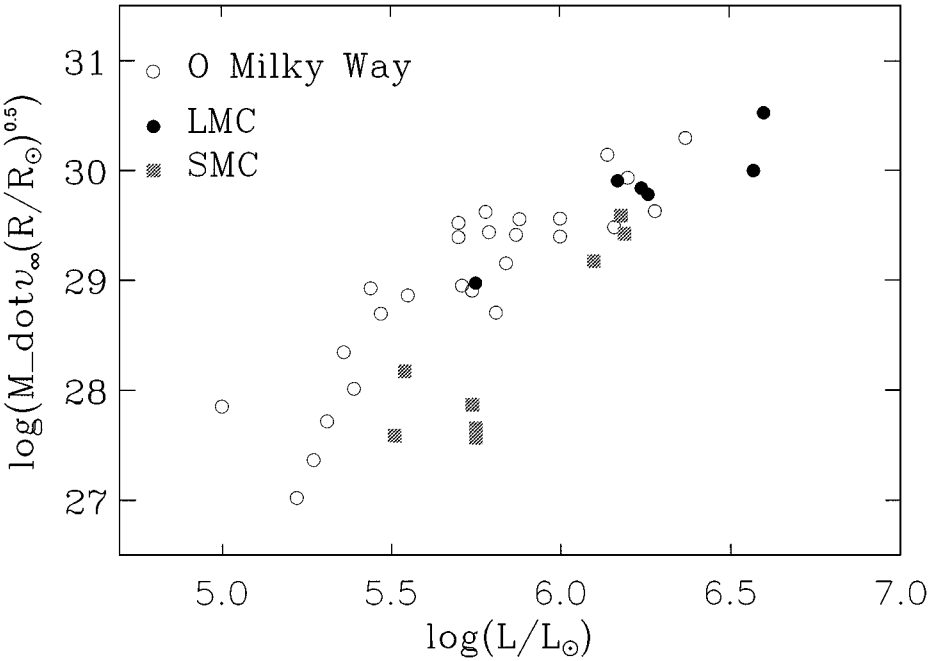


**Figure 11** Wind momenta of O-stars in the Galaxy, LMC, and SMC as a function of luminosity. Data from Puls et al (1996).



and 5. Introducing the "line-strength" $k_i$ and the Thomson optical depth parameter $t(r)$, the optical thickness $\tau_i$ of each line can be expressed as

$$k_i = \frac{n_l}{n_e \sigma_e v_{\rm therm}} f_{lu} \lambda_i, \quad t(r) = n_e \sigma_e \frac{v_{\rm therm}}{{\rm d}v/{\rm d}r} \frac{R_*}{v_\infty}, \quad \tau_i = k_i t(r). \qquad (11)$$

$t(r)$ corresponds to the local optical thickness of a line for which the integrated line opacity is just equal to the one of Thomson scattering. The line-strength $k_i$ measures line opacities in units of Thomson scattering (neglecting stimulated emission). Whether a line is optically thick or thin at a certain point in the wind depends on the line strength as well as on the local hydrodynamical situation. Optically thin and thick lines contribute to the radiative acceleration $g_{\rm rad}^{\rm lines}$ in a completely different way (for a detailed discussion of the following formulae, see, for instance, Kudritzki 1988, 1998; Puls et al 2000):

$$g_{\rm rad}^{\rm thin} \propto \frac{k_i}{r^2}, \qquad g_{\rm rad}^{\rm thick} \propto \frac{1}{r^2 \rho} \frac{{\rm d}v}{{\rm d}r}. \qquad (12)$$

It is, therefore, crucial to know the contribution of optically thick and thin lines throughout the wind, which can be accomplished in an elegant way by introducing a line-strength distribution function. In the theory of radiation-driven winds, such

a distribution function can be calculated from the opacities of the hundreds of thousands of lines driving the wind. It turns out to be a power law in line strength (for a comprehensive discussion of the physics of the line-strength distribution function, see Puls et al 2000):

$$n(k_i)\,\mathrm{d}k_i \propto k_i^{\alpha-2}\,\mathrm{d}k_i, \qquad 1 \le k_i \le k_i^{\max}. \tag{13}$$

The exponent $\alpha$ of the line-strength distribution function is crucial for the calculation of the total radiative line acceleration, which (after integration over line strength) finally becomes

$$g_{\mathrm{rad}}^{\mathrm{lines}} \propto N_{\mathrm{eff}} \frac{1}{r^2} t^{-\alpha}, \tag{14}$$

with $N_{\mathrm{eff}}$ the number of lines effectively driving the wind. This means that the line acceleration depends nonlinearly on the velocity gradient. However, for $\alpha = 0$, we would recover the optically thin case, whereas $\alpha = 1$ would correspond to the optically thick case. For O-stars, a typical value is $\alpha \sim 2/3$.

The local non-LTE ionization balance in a stellar wind depends on the ratio of electron density to the geometrically diluted radiation field (see Section 2.4.1) and may change from the photosphere to the outer layers of the stellar wind flow. In such a case we would also expect the line-strength distribution function to change so that both $\alpha$ and $N_{\mathrm{eff}}$ vary with height. Abbott (1982) introduced a parameterization of this effect by adopting $N_{\mathrm{eff}} = N_0(10^{-11}\mathrm{cm}^3 n_e/W)^{\delta}$, with electron density $n_e$ (in cgs units) and dilution factor $W$. This parameterization accounts only for ionization changes in the normalization ($N_{\mathrm{eff}}$) of the line-strength distribution function, but it ignores possible simultaneous effects on its slope ($\alpha$), which can become important under certain conditions (see Kudritzki et al 1998, Puls et al 2000). Typical values of $\delta$ for O-stars are $\delta \sim 0.05$–$0.1$.

## 4.1 Nonrotating Winds

Solving the equation of motion for stationary, spherically symmetric line-driven winds with line-strength distribution functions as described by Equations 13, the $\delta$ term, and corresponding radiative line accelerations (Equation 14), one obtains for terminal velocity and the mass-loss rate (see Kudritzki et al 1989)

$$v_\infty = 2.25 \frac{\alpha}{1-\alpha} v_{\mathrm{esc}}\, f_1(\alpha)\, f_2(\delta)\, f_3(v_{\mathrm{esc}}) \tag{15}$$

and

$$\dot{M} \propto N_0^{\frac{1}{\alpha'}}\, L^{\frac{1}{\alpha'}}\, (M_*(1-\Gamma))^{1-\frac{1}{\alpha'}}, \quad \alpha' = \alpha - \delta. \tag{16}$$

The functions $f_1$, $f_2$, $f_3$ are of the order of unity and are obtained from numerical fits to the results found by Kudritzki et al (1989),

$$f_1(\alpha) = \frac{8}{5}\left(1 - \frac{3}{4}\alpha\right), \qquad f_2(\delta) = e^{-2\delta}, \quad f_3(v_{\mathrm{esc}}) = 1 - 0.3e^{-\frac{v_{\mathrm{esc}}}{300\,\mathrm{km/s}}}. \tag{17}$$

Equation 15 demonstrates that the theory of line-driven winds does indeed lead to a proportionality of $v_\infty$ to $v_{\rm esc}$ (the influence of $f_3$ is small), as indicated by the observations. The ratio $v_\infty/v_{\rm esc}$ does obviously depend on the value of $\alpha$, the power law exponent of the line-strength distribution function. This means that the physical nature of the lines driving the wind such as ionization stages, chemical composition, etc, is fundamentally important. A steep line-strength distribution function (small $\alpha$, many weaker lines) will produce a slow wind, whereas a flatter function (large $\alpha$, more stronger lines) will lead to a faster wind.

The mass-loss rate is influenced by both the effective number of lines $N_0$ driving the wind and the slope $\alpha'$, in particular, because of its dependence on the stellar luminosity. Unfortunately, $\dot{M}$ depends also on the "effective mass" $M_*(1-\Gamma)$, which, for instance for O-stars and early B-supergiants, varies greatly from star to star and introduces a significant scatter, if one wants to correlate stellar mass-loss rates with luminosity.

The scatter is, however, reduced if one considers the "modified stellar wind momentum," as introduced by Equation 10 and combines Equations 15, 16, and 8 to obtain

$$D_{\rm mom} = \dot{M} v_\infty (R_*/R_\odot)^{0.5} \propto N_0^{\frac{1}{\alpha'}} L^{\frac{1}{\alpha'}} (M_*(1-\Gamma))^{\frac{3}{2}-\frac{1}{\alpha'}}. \qquad (18)$$

The absolute value of the exponent of the effective mass is now smaller, reducing the influence of this quantity, in particular for O-stars and early B-supergiants, where the theory predicts a value of $\alpha = 2/3$ (see Puls et al 2000). This is the reason why an analysis of observed stellar wind momenta is more straightforward than a discussion of mass-loss rates. Equation 18 is the basis for the concept of the wind momentum–luminosity relationship (WLR) (see Equation 10), as introduced by Kudritzki et al (1995) and Puls et al (1996) (see Kudritzki 1998, for a simplified derivation of Equation 18).

The slope of the observed WLR can be used to determine the value of $\alpha'$ empirically as a function of the spectral type through $\alpha' = 1/x$. The corresponding values are given in Table 2 and indicate that $\alpha'$ decreases systematically with decreasing effective temperature. This conclusion is confirmed by applying Equation 15 to the observed ratios $v_\infty/v_{\rm esc}$ (see Equation 9). Assuming $\delta = 0.05$ and $v_{\rm esc} = 700, 350$, and 200 km/s for O-stars, B-supergiants with $T_{\rm eff} \leq 22{,}000$ K, and A-supergiants, respectively, we obtain for $\alpha$ 0.60, 0.40, and 0.32, slightly lower than the values in Table 2 but indicating the same trend with $T_{\rm eff}$ (see also Lamers et al 1995, Achmad et al 1997, who were the first to point out that the terminal velocities of A- and mid-to-late B-supergiants require low values of $\alpha$).

The physical reason for the change in the slope of the line-strength distribution function with effective temperature is, of course, the change in ionization of the elements contributing to the radiative line acceleration. As shown in the detailed investigation by Puls et al (2000), changes of ionization affect the line-strength distribution function mostly at small and intermediate line strengths. Here, the contribution of the iron group elements is crucial with their large number of metastable levels. With decreasing ionization, the number of lines from iron group

elements at small and intermediate line strengths becomes larger and larger. On the other hand, the contribution to the line-strength distribution at large line strengths results mostly from light ions, whose contribution remains rather constant, as a function of temperature. As a result, the slope of the total line-strength distribution function over all line strengths becomes steeper and $\alpha$ becomes smaller with decreasing effective temperature.[3] The effect is, thus, understood qualitatively. A quantitative confirmation based on a detailed comparison at the low-temperature end of non-LTE wind models with observations resulting from the spectroscopic analysis has still to be carried out [see, however, first results presented by Kudritzki (1999a,b)].

The variation of the coefficient $D_0$ of the WLR can be used to estimate empirically the effective number of lines $N_0$ contributing to the stellar wind acceleration. This is, however, a more complex matter because $D_0$ depends on the flux-weighted total number of spectral lines as well as on $\alpha'$ and $\alpha$ itself (Puls et al 2000). Only in cases of similar slopes does a comparison give direct insight into the absolute number of effectively driving lines, whereas in all other cases their distribution with respect to line-strength ($\alpha$) has a significant influence on the offset.

Because of its (partial) dependence on flux-weighted line number, $D_0$ varies between spectral types not only because of ionization changes, but also because of the different spectral locations of the lines with regard to the flux maximum and absorption edges, such as the hydrogen Lyman and Balmer edges. At least concerning the observed differences in $D_0$ between O-type and A-type supergiants (accounting for the changes in $\alpha'$), $D_0$ can be understood in terms of the theoretically predicted effective number of lines $N_0$, as demonstrated by Puls et al (2000). However, to predict the full variation of $D_0$ over the whole range of effective temperatures quantitatively, and thus to check whether this interpretation is generally valid, will require more detailed calculations of radiation-driven wind models. As expressed by Kudritzki et al (1999), the pronounced drop in $D_0$ between effective temperatures of 23,500 K and 22,000 K (on the temperature scale of unblanketed models) is a particular challenge for the theory. A detailed spectroscopic study of a larger sample of objects in this transition range of temperatures to disentangle stellar wind properties in more detail will certainly be valuable. In addition, a careful reinvestigation into whether systematic effects (for instance, deviations of the helium abundances from the normal value, or metal line blanketing and blocking in this temperature range) may have influenced the results of the spectroscopic analysis will be important.

The theory of line-driven winds also makes a clear prediction about the influence of metallicity on the strengths of stellar winds. The first-order effect arises from the fact that the effective number of lines contributing to the line acceleration changes

[3]We note in passing that the power law fit of the line-strength distribution function with a constant exponent $\alpha$ is only a first-order approximation. In reality, the function shows a distinct curvature, which must be considered in realistic stellar wind calculations (see Pauldrach et al 1994, Kudritzki et al 1998).

with metallicity $\epsilon$ and, hence, causes a metallicity dependence of the mass-loss rate

$$N_0(\epsilon) = N_0^{\odot}\,(\epsilon/\epsilon_{\odot})^{1-\alpha}\,, \qquad \dot{M}(\epsilon) = \dot{M}(\epsilon_{\odot})\,(\epsilon/\epsilon_{\odot})^{\frac{1-\alpha}{\alpha'}}\,. \tag{19}$$

Taking values of $\alpha'$ from Table 2 and adopting $\delta = 0.05$, we obtain exponents for the metallicity dependence of mass-loss rates of the order of 0.5, 0.8, and 1.7 for O-stars (and early B-supergiants), mid B-supergiants, and A-supergiants, respectively. Theoretical stellar wind calculations by Kudritzki et al (1987) and Leitherer et al (1992) confirm the numbers for the first two cases. The only observational test so far results from Puls et al (1996), which in the metallicity range between the Galaxy and the SMC ($\epsilon \sim \epsilon_{\odot}/5$) confirms the exponent of 0.5 for O-stars. Whether the very strong metallicity dependence predicted for A-supergiants is really observed needs to be checked by a systematic analysis of winds of those objects in the SMC. The work by McCarthy et al (1995), where the analysis of a very-metal-poor A-supergiant in the outskirts of M33 leads to a very small mass-loss rate, indicates that the large exponent might be appropriate.

A second effect might be important for the metallicity dependence of terminal velocities as well as for the overall slope ($x = 1/\alpha'$) of the WLR, as discussed by Puls et al (2000). This effect results from the curvature of the line-strength distribution function, which has a steeper slope (smaller $\alpha$) for the larger line strengths, which become important for the acceleration of winds at lower metallicity, where the winds are weaker and the corresponding optical thicknesses are smaller. However, as pointed out by Puls et al, there are several competing effects of comparable magnitude in the acceleration of the outer layers of winds, such as differences in CNO abundance ratios or changes in ionization at different metallicity. It is, therefore, too early to make a clear theoretical prediction for all spectral types. The lower terminal velocities (as well as the indications of a steeper slope) observed for SMC O-stars, though, indicate that the theory is appropriate for O-stars.

### 4.1.1 The Problem of Thin Winds

As we have seen (cf Figure 8), the observed WLR for O-type dwarfs, if taken literally, exhibits a severe curvature toward (very) low wind momenta at luminosities lower than $\log L/L_{\odot} = 5.3$. (Note that the derived momenta are upper limits in this luminosity range.) As pointed out above, the two objects that fall below the relation are rapid rotators. Although this fact alone might initiate the deviations from the WLR (see the next subsection), there are three additional effects that are important for the physics of very thin winds from dwarfs (or in a low metallicity environment) and might induce a strong deviation from the usual WLR.

First, standard theory requires the photon momentum absorbed almost exclusively by metal ions to be transferred to the bulk of the wind plasma (hydrogen and helium) via Coulomb collision. A detailed investigation by Springmann & Pauldrach (1992) illuminated the limits of this process: For thin winds, the metal ions can decouple from the rest of the plasma, and the wind no longer reaches the

same terminal velocity that would follow in the standard picture. Using a multifluid approach (including the various Coulomb collisions as function of plasma parameters), Babel (1995) presented a model for inhomogeneous radiatively driven winds of A-dwarfs, where the resulting $\dot{M}$ turned out to be very low. Second, the inclusion of shadowing by photospheric lines (not considered in the usual computation of the line force) has large consequences for the wind of B-dwarfs, resulting again in mass-loss rates well below the standard results (Babel 1996). Finally, as shown by Puls et al (1998) and Owocki & Puls (1999), curvature terms of the velocity field in the transonic region can lead to line accelerations much smaller than in the standard computations, leading to reduced mass-loss rates. This process, however, is only effective when the continuum is optically thin throughout the transonic region, i.e., it can be present only in thin winds. Together, these results imply that low-luminosity dwarfs are subject to a number of processes reducing the mass-loss rate compared with the scaling relations above. The position of the turnover point as a function of various stellar parameters (including metallicity), however, remains to be defined.

## 4.2 Influence of Rotation

So far, our discussion has neglected the influence of rotation on the wind structure itself. This is discussed below. Recent reviews on this topic have been given by Owocki et al (1998a,b), Bjorkman (1999), and Puls et al (1999). [For the effects of rotation on stellar evolution/structure, see Langer & Heger (1998), Maeder (1998, 1999), and Meynet (1998).]

The major aspect that has to be accounted for in addition to the "conventional" approach, at least at first glance, is the impact of centrifugal acceleration as a function of radius $r$ and co-latitude $\theta$. It was studied first by Friend & Abbott (1986) and Pauldrach et al (1986) in its most simple way, considering only particles in the equatorial plane. With the assumption of a purely radial line acceleration, the angular momentum remains conserved (only central forces present), and the rotational speed is given by $v_\phi(r) = v_{\rm rot}(R_*, \theta = \pi/2)/r$. Thus, the usual equation of motion is modified by the centrifugal acceleration only, which leads to an effective gravity of $GM(1-\Gamma)/(R_* r)^2(1-\Omega^2/r)$, where $\Omega$ is the ratio of rotational speed at the (equatorial) surface $v_{\rm rot}(R_*)$ to the break-up velocity $v_{\rm break} = v_{\rm esc}/\sqrt{2}$, with $v_{\rm esc}$ the photospheric escape velocity defined in Equation 8. Thus, the only difference to nonrotating models is the modification of effective mass by roughly a factor of $(1-\Omega^2)$:

$$\dot{M}(\Omega) = \dot{M}(0)(1-\Omega^2)^{1-1/\alpha'}; \quad v_\infty(\Omega) = v_\infty(0)(1-\Omega^2)^{\frac{1}{2}}. \qquad (20)$$

$\dot{M}(0)$ is the mass-loss rate without rotation (cf Equation 16), and the second relation follows from the scaling properties of the terminal velocity, $v_\infty(\Omega = 0) \propto v_{\rm esc}$ (Section 4.1). [A more elaborate version of the latter expression has been given by Puls et al (1999).] A comparison of both scaling laws with hydrodynamical simulations shows a satisfying agreement.

Of course, the above scaling laws are valid only in the equatorial plane and can be considered as sort of a maximum effect. Accounting also for the variation of $v_\phi$ as a function of $\theta$, Bjorkman & Cassinelli (1993) elaborated on the concept of so-called wind-compressed disks and zones.

The basic idea follows again from the assumption of purely radial line forces. Thus, the specific angular momentum is actually conserved for all particles, and their motion is restricted to the orbital plane to which they belong (tilted by an angle of co-latitude $\theta_o$ from which they start). Neglecting pressure forces in the supersonic region, the free flow of the particles can be simulated then by a corresponding 1-D treatment, as above, with modified rotational rate $\Omega \sin\theta_o$. Consequently, mass-loss rates and velocities in the orbital plane follow the same scaling relations as above, however with $\Omega^2$ replaced by $\Omega^2 \sin^2\theta_o$. In the course of the particles' motion, their azimuthal angle $\Phi'(r)$ in the orbital plane is increasing, and they are deflected toward the equator. If the ratio of $v_{\rm rot}/v_\infty$ is significant and/or the radial velocity field in the lower wind region is flat, $\Phi'$ might become $\geq \pi/2$, and the particles would cross the equator. Here, they collide supersonically with particles from the other hemisphere, and a wind-compressed disk (WCD) is formed. In those cases where the particles do not collide ($\Phi'(r \to \infty) < \pi/2$), at least a wind compressed zone (WCZ) is created, i.e. an anisotropic wind with highest densities at the equator.

The hydrodynamical stratification in stellar coordinates is obtained by following the particles' stream lines. For noncolliding winds with not too large deflection angle $\Phi'$ or generally close to the star ($\theta \approx \theta_o$), one finds

$$\dot{M}(\theta) \approx \dot{M}(0)(1-\Omega^2 \sin^2\theta)^{1-1/\alpha'}; \qquad v_\infty(\theta) = v_\infty(0)(1-\Omega^2 \sin^2\theta)^{\frac{1}{2}}, \quad (21)$$

i.e. $\dot{M}$ increases and $v_\infty$ decreases toward the equator. Further consequences are discussed by Bjorkman & Cassinelli (1993) and Bjorkman (1999), and the validity of the WCD-model has been confirmed in principle by Owocki et al (1994) on the basis of time-dependent hydrodynamical simulations.

It is important to realize that the outlined results rely exclusively on the assumption of purely radially directed line forces. As determined by a detailed investigation of the other (vector) components (cf Owocki et al 1996), the polar one in particular cannot be neglected in the delicate balance of forces[4]. As long as the radial velocity law at the equator is slower than in polar regions—an almost inevitable consequence of rotation due to the reduced escape velocity at the equator—a pole-ward acceleration is created that is sufficient to stop the equatorward motion predicted by WCD/WCZ models and actually reverses its direction, an effect called the "inhibition effect": Disks can no longer be formed. Together with the distortion of the stellar surface by centrifugal forces (e.g. Cranmer & Owocki 1995) and the well-known von Zeipel theorem (surface flux scaling with effective gravity as a function of $\theta$) (for recent improvements, cf Maeder 1998,

[4]Concerning the azimuthal component affecting the angular momentum and allowing for a spin-down of the wind, cf Grinin (1978) and Owocki et al (1998a).

1999) the original scaling of $\dot{M}$ (Equation 21) can be actually reversed, i.e. the inclusion of gravity darkening (increased polar radiation flux) might lead to a larger polar mass flux

$$\dot{M}(\theta) \propto (1 - \Omega^2 \sin^2\theta)^{+1} \quad \text{with gravity darkening} \tag{22}$$

(cf. Owocki et al 1998a,b).

Recent work by Petrenz (1999) concentrated on a consistent description of hydrodynamics and statistical equilibrium (controlling the line force) in order to clarify how important the 2-D stratification of occupation numbers is and how much influence it might have on the final result. A number of models with various kinds of differing approximations have been calculated, confirming however all basic trends quoted above.

Thus, the current status of modeling rotating stellar winds can be summarized as follows: If one neglects the nonradial components of the line force, an oblate wind structure is created, with meridional velocities directed toward the equator. For large values of $\Omega$, a WCD might show up. Accounting additionally for nonradial line forces, the resulting pole-ward acceleration reverts the direction of the meridional velocity field and "inhibits" the disk formation. Finally, the inclusion of gravity darkening allows even for a prolate wind structure.

In view of these different scenarios [for additional processes that might be relevant, cf Bjorkman (1999)] and with respect to our discussion of the WLR, it is especially interesting to investigate the dependence of wind momentum on rotation. From the simplified approach (Equation 21) and for $\alpha' = 2/3$, the wind-momentum rate becomes independent of angle, i.e., $\dot{M} v_\infty(\Omega, \theta) \approx \dot{M} v_\infty(\Omega = 0)$,because as in the corresponding 1-D models, the dependence on effective mass completely cancels out. Numerical simulations (radial forces only) verify this prediction with high accuracy (P Petrenz, private communication). The maximum influence, on the other hand, and discarding disks, is obtained for models with nonradial forces and gravity darkening. For large values of $v_{\rm rot}$(250 . . . 350 km/s), the wind-momentum rate varies typically by a factor of 2 (pole) to 0.5 (equator), compared with 1-D, nonrotating models. Because $\dot{M}$ and $v_\infty$ depend on $\Omega^2$, the effect of "normal" rotational rates, however, becomes minor with respect to other uncertainties. Note especially that all theoretical results derived so far unfortunately lack direct observational proof.

There exists another class of massive objects where rotation might be even more important: the B[e]-supergiants with a well-determined bimodal structure (slow and dense equatorial wind and fast, thin polar wind) (for a recent review, see Zickgraf 1999). As has been shown by Pauldrach & Puls (1990) and investigated in detail by Vink et al (1999), continuum optical depth effects in the B-supergiant domain can induce the so-called bi-stability mechanism. The decisive quantity that controls this behavior is the optical depth in the Lyman continuum, which—for rotating stars and accounting for gravity darkening—depends sensitively on rotationally induced variations of wind density and radiation temperature and thus

becomes a strongly varying function of $\theta$ (Lamers & Pauldrach 1991, Lamers et al 1999b; but see also Owocki et al 1998a). Because of this behavior, the bistability effect is thought to be responsible for the B[e] phenomenon (Lamers & Pauldrach 1991) if the star rotates close to break-up and has a large average mass loss. First hydrodynamical simulations (Petrenz 1999; HJGLM Lamers, private communication) indicate that this hypothesis might actually work.

## 5. TIME DEPENDENCE AND STRUCTURE

The basic philosophy underlying the previous results and conclusions has been outlined in Section 2.2 and comprises the assumption of a globally stationary wind (1-D or 2-D) with a smooth density/velocity stratification. However, as follows directly from the assumption of stationarity, these models are inherently incapable of describing a number of observational features (partly referred to in Section 2.4), which immediately show that nonstationary aspects of the wind must be important. Moreover, theoretical considerations based on a detailed investigation of the wind-driving agent, radiative-line acceleration, show clearly that this acceleration is subject to a strong instability, which, when "allowed" to operate in time-dependent models, causes a variable and strongly structured wind hardly resembling the stationary and smooth model underlying our philosophy, at least at first glance. This section outlines the status quo with respect to observations and theory and some further implications.

### 5.1 Observational Findings

In our review of diagnostic methods to derive global wind parameters (Section 2.4) we have met a number of issues that are difficult to reconcile with the stationary/smooth picture of winds. The following enumerations summarize the most important observational findings concerning structure and temporal variability (including those already mentioned); for further details we refer to the proceedings cited at the end of Section 2.2.

(*a*) Soft X-ray emission from hot stars is attributed to randomly distributed shocks in their winds. It is required to model the observed degree of superionization (cf Section 2.4.5). (*b*) Nonthermal radio emission is observed for roughly 30% of massive stars and may be interpreted as synchrotron radiation from first-order Fermi-accelerated electrons, requiring again the presence of shocks (cf Section 2.4.4). (*c*) Black troughs in saturated P-Cygni profiles are simulated by a velocity dispersion in the stationary description. However, a better physical basis for interpreting them is as a consequence of backscattering in multiply nonmonotonic flows (cf Section 2.4.1). (*d*) Electron-scattering wings of recombination lines in Wolf-Rayet stars are weaker than predicted by smooth models, which suggests the possibility of a clumped structure (Hillier 1991). WR models accounting for the effects of clumping succeeded in producing perfect line fits, with the implication of

reduced (factor of 2) mass-loss rates (Schmutz 1997, Hamann & Koesterke 1998). (*e*) The inconsistency of IR-excess and radio flux for a small number of objects can be resolved if clumping is accounted for (Section 2.4.4). (*f*) Variability is observed in optical wind lines such as $H_\alpha$ (Ebbets 1982) and HeII $\lambda$ 4686 (Grady et al 1983, Henrichs 1991), both for OB-stars as well as for BA-supergiants (Kaufer et al 1996). Minimum timescales are of the order of hours, i.e. wind-flow times. (*g*) Direct evidence (from HeII $\lambda$ 4686) for outmoving inhomogeneities (e.g. clumps, blobs, or shocks) is reported for the wind of $\zeta$ Pup (Eversberg et al 1998). The spectropolarimetric variations detected by Lupie & Nordsieck (1987) in a sample of 10 OB-supergiants also provide direct evidence of inhomogeneous wind structure.

Predominantly photospheric lines such as HeI $\lambda$ 5876 are found to be variable as well (Fullerton et al 1992), and in a spectroscopic survey of a large sample of O-stars by Fullerton et al (1996), 77% of the stars investigated (all supergiants of the sample and few dwarfs later than O7) showed photospheric line profile variability with an amplitude increasing with radius and luminosity, likely related to nonlinear stellar pulsations. (*h*) Variability is observed as well in UV P-Cygni lines, where the blue edges vary most significantly, whereas the red emission part remains relatively constant (Henrichs 1991, Prinja 1992). $H_\alpha$ and UV variability on the one hand (Kaper et al 1997) and $H_\alpha$ and X-ray variability on the other (Berghöfer et al 1996) seem to be correlated and might indicate the propagation of disturbances throughout the entire wind. (*i*) Discrete absorption components (DACs) are among the most intensively studied manifestations of wind variability and structure in OB-stars. These features are optical depth enhancements that accelerate through the absorption troughs of unsaturated P-Cygni profiles from low to high velocities much more slowly than the mean outflow (e.g. Prinja et al 1992). Lamers et al (1982) reported the presence of narrow components in 17 of 26 OB-stars at a blue velocity of $0.75 v_\infty$ and discussed the presence of velocity plateaus as one of a number of possible explanations. Later studies (e.g. Henrichs 1984, Prinja & Howarth 1986) revealed that P-Cygni lines also vary at lower velocities, although over a broader velocity range. Extensive time series (Prinja et al 1987, Prinja & Howarth 1988) have shown that these broad features evolve into the high-velocity narrow components on timescales of a few days. Both features were "unified" in terms of DACs. Note that Howarth & Prinja (1989) and Prinja et al (1990) used the narrow absorption features to determine $v_\infty$ for those objects with no black trough in CIV (cf Section 2.4.1).

Reviews of the phenomenology associated with DACs have been given by Howarth (1992), Prinja (1992), Henrichs et al (1994), and Kaper & Henrichs (1994). The latest results (also in connection with the modulation features described below) have been reported by Kaper et al (1999). Note that DACs are found not only in O- and early B-stars, but also in B-supergiants as late as B9 (Bates & Gilheany 1990) and in at least one WN7-star (Prinja & Smith 1992).

Although the nature of the DACs is still unclear, the finding that their acceleration and recurrence time is correlated with the stellar rotational period [actually,

faster-developing, more frequent DACs are apparent in stars with higher $v_{\rm rot} \sin i$ (cf Prinja 1988, 1992; Henrichs et al 1988, Kaper 1993)] turned out to be important not only by itself, but also because it inspired the "IUE MEGA Campaign" (Massa et al 1995). During 16 days of nearly continuous observation with IUE, three prototypical stars [$\zeta$ Pup (O4If ), HD 64760 (B0.5Ib), and HD 50896 (WN5)] were monitored in order to assess the presumed correlation of rotation versus wind activity. The results of this campaign (together with other observational runs) have recently been summarized by Fullerton (1999). For $\zeta$ Pup, one of the derived periods [from SiIV (cf Howarth et al 1995)] is within the uncertainties associated with the rotational period; however its wind appears to be subject to a variety of perturbations. The analysis of the time series for HD 64760 (Prinja et al 1995) lead to the detection of a new type of variability, namely periodic modulations in the UV wind lines. Fullerton et al (1997) have shown that these modulations result from two quasi-sinusoidal fluctuations with periods of 1.2 and 2.4 days and can be traced throughout the emission part of the profiles, i.e. they must be caused by longitudinally extended structures. The modulations develop simultaneously toward lower and higher velocities, an effect called "phase bowing," which has been explained by co-rotating, spiral-shaped wind structures (Owocki et al 1995). These structures might be identified with so-called corotating interaction regions (CIRs) caused by the collision of fast and slow winds that emerge nearly radially from different longitudinal sectors of the stellar surface. CIRs have long been studied in the solar wind and were first proposed by Mullan (1984, 1986) as an explanation for the DACs in OB-star winds. Actually, Cranmer & Owocki (1996) have suggested that CIRs are responsible not only for the modulation features but also for the "classical" DACs (thus supporting the suggestion by Mullan) by creating velocity plateaus in the wind [see also the early suggestion by Lamers et al (1982)]. With respect to this explanation, however, a number of problems related to the treatment of the line force in the hydrodynamic simulations are still unresolved (Owocki 1999).

## 5.2 Theoretical Considerations

Theoretical efforts to understand the nature and origin of these observational findings have generally focused on the line-driving mechanism itself. Linear stability analyses on the basis of a non-Sobolev description (see below) have shown the line force to be highly unstable (MacGregor et al 1979; Carlberg 1980; Abbott 1980; Lucy 1984; Owocki & Rybicki 1984, 1985), with inward-propagating waves being more strongly amplified than outward-propagating ones.

Initial heuristic models by Lucy & White (1980) and Lucy (1982a) assumed that the resulting wind structure would consist of a periodic train of forward shocks. With some adjustment of parameters, this model reproduced the observed flux of soft X-rays (Lucy 1982b), although not the hard X-ray tail (Cassinelli & Swank 1983). Lucy (1982a, 1983) further showed that the multiply nonmonotonic nature of the resulting velocity field could explain the black absorption troughs observed in saturated UV resonance lines (cf Section 2.4.1).

Subsequent efforts have focused on dynamical modeling of the time-dependent wind structure from direct, numerical simulation of the nonlinear evolution of the line-driven flow instability (for reviews see Owocki 1992, Owocki 1994, Feldmeier 1999). The key aspect regards the computation of the force itself because, for unstable flows with structure at scales near or below the Sobolev length (Section 2.4.1), a local approach as given by the Sobolev treatment inevitably fails unless very refined precautions are taken (Feldmeier 1998). Instead, one must apply complex, computationally expensive integral forms that take into account the nonlocal character of radiation transfer. Owocki & Puls (1996, 1999) have discussed various levels of approximations that both account for the key effects and are computationally feasible.

The most important finding of the first simulations by Owocki et al (1988) was that the nonlinear evolution leads to strong reverse shocks, a robust result that follows directly from the much stronger amplification of inward-propagating waves (see above). So-called smooth source function models (Owocki 1991) based on a simple approximation to incorporate the potentially stabilizing effect of the "line-drag" by the diffuse, scattered radiation field (Lucy 1984, Owocki & Rybicki 1985) have proven to be significantly more stable than the first models based on pure absorption, particularly in the lower wind. The outer wind, however, still develops extensive structure that consists, as before, of strong reverse shocks separating slower, dense shells from high-speed rarefied regions in between: Only a very small fraction of material is accelerated to high speed and then shocked; for most of the matter, the major effect is a compression into narrow, dense "clumps" (shells in these 1-D models), separated by large regions of much lower density.

Feldmeier (1995) extended these models by relaxing the assumption of isothermality, accounting for the energy transport, including radiative cooling. By investigating the influence of various photospheric disturbances that induce the onset of structure formation (via exciting the line-force instability), Feldmeier et al (1997b) concluded that cloud-cloud collisions [and not the cooling of the reverse shocks themselves (e.g. Cooper & Owocki 1992)] are the actual reason for the observed X-ray emission (cf Section 2.4.5).

Current effort concentrates on 2/3-D simulations of winds in order to clarify the effects of rotation (cf Section 4.2) as well as the role of the line instability with respect to CIR models (Section 5.1). Owocki (1999) has given some impressive, however preliminary, results of first simulations, which indicate that the small-scale, intrinsic line instability can completely disrupt any kind of large-scale structure if it becomes too strong, as seems to be the case for the current model generation.

## 5.3 Implications with Respect to Global Parameters

Obviously, time-dependent models based on a nonlocal line force provide a satisfying explanation for a large number of observational findings. The results with

respect to X-ray emission are most promising, and the presence of shocks also allows construction of a consistent description of nonthermal radio emission in winds from single stars. Because the latter scenario requires shocks that have survived until large radii, it seems at least plausible that only a fraction of massive stars are seen as nonthermal emitters (cf Chen & White 1994).

One the other hand and at first glance, these models appear to be in strong contrast with our assumptions for the standard model for wind diagnostics based on stationarity and homogeneity, especially when viewed with respect to the spatial variation of velocity and density. However, when viewed with respect to the mass distribution of these quantities, the models are not so very different (Owocki et al 1988, Owocki 1992, Puls et al 1993a). Furthermore, gross wind properties, such as terminal flow speed and time-averaged mass-loss rate, turn out to be in good agreement with those following from a stationary approach [despite the problem of (very) thin winds] (cf Section 4).

Given the intrinsic mass weighting of spectral formation (at least for resonance lines with constant ionization fraction) and the extensive temporal and spatial averaging involved, the observational properties of such structured models may be similar to what is derived from the "conventional" diagnostics, in an average sense. In detailed line-formation calculations assuming line opacities proportional to the local density, Puls et al (1993a, 1994) and Owocki (1994) showed that this conjecture is actually justified, and they were able to demonstrate that unstable winds are excellent candidates for explaining the observed black troughs.

In summary, such models seem able to offer the possibility of retaining the successes of stationary models in matching time-averaged observational properties, while also reproducing the spectral signatures (X-rays, nonthermal radio emission, black troughs, first hints on the nature of DACs, and modulation features), which suggests the existence of extensive wind structure.

However, as should be clear from Section 2.4, only part of the described diagnostic methods relies on features coupled to processes with opacities $\propto\rho$. The determination of $\dot{M}$ (and $\beta$) depends on opacities/emissivities $\propto\rho^2$, regardless of whether it is determined via $H_\alpha$, IR excess, radio fluxes, or SiIV resonance lines [in so far as the calibration of mean ionization fractions of SiIV to radio and $H_\alpha$ mass-loss rates (Section 2.4.1) is intrinsically consistent!], so that the assumption of a stationary wind without clumping seems questionable in view of the perspectives outlined above.

Let us first concentrate on the results derived from $H_\alpha$, the primary diagnostic tool also for extragalactic work. At least for the majority of OB-stars, the corresponding wind emission comes from lower wind layers, typically between 1.0 and 1.5 stellar radii. Hydrodynamical simulations of self-excited wind instabilities show that these layers seem to be unaffected by shocks and that instabilities only occur further out in the wind (Owocki 1994). This agrees with the fact that the observed X-rays most probably are emitted in the outer layers (Hillier et al 1993) and that the black troughs considered above can arise also from small-scale structures present only in the outer wind (see also Owocki 1994).

Nevertheless, instabilities producing a small-density contrast might still be present in the $H_\alpha$ forming region, if the wind is triggered by photospheric perturbations [sound waves, (non)radial pulsations], in accordance with observational findings that disturbances (of low amplitude) are seen throughout the wind (Section 5.1). In such cases, the location of the onset of structure formation depends crucially on the damping by the diffuse radiation force. Recent hydrodynamical simulations including photospheric perturbations (Feldmeier et al 1997b) show pronounced inhomogeneous structures only above 1.3 $R_*$, and even in the most elaborate models, including the effects of disturbances in the diffuse radiation field (Owocki & Puls 1999), the same result is found. Thus it seems probable that the neglect of clumping does not induce large systematic errors for OB-star mass-loss determinations. For A-supergiants, the situation remains unclear because hydrodynamical simulations in the corresponding parameter space have yet not been performed and because the lines are formed all the way out to larger radii.[5]

A second line of reasoning in favor of our assumption was given by Lamers & Leitherer (1993) and Puls et al (1993b). Briefly, they argued that because of the same $\rho^2$ dependence of both the radio and the $H_\alpha$ emission and the fact that both rates agree for those objects with $H_\alpha$ and radio mass-loss rates, this would imply the same clumping factor in regions close to $H_\alpha$ and far away from the star (radio). As this is rather unlikely because in the lower wind the formation of structure just sets in, whereas in the outer part any structure should have stabilized, it is probable that the degree of clumping in the lower wind part is small, if present at all. A scenario consistent with all observational facts has been described by Feldmeier et al (1997b), based on a simulation extended to 100 stellar radii: The lower wind remains rather smooth (damping of the instability), the intermediate part is clumpy (line-force instability "at work"), and the outermost part (above 10 $R_*$) is rather smooth again, related directly and indirectly to inefficient radiative cooling in this region. Note, however, that a few strong shocks actually survived up to large radii in this model, just as required to produce nonthermal radio emission.

As a consequence of this scenario, one would expect erroneous mass-loss rates only from diagnostics of the intermediate wind part, in accordance with the findings of an inconsistency of IR excess and radio mass-loss rate from a few stars described by Runacres & Blomme (1996) and the discrepancy for the mass-loss rate of HD 53138 discussed in Section 2.4.4.

If, in contrast, one were to assume the worst case of significant structure everywhere in the wind, this would imply that all current results from refined non-LTE diagnostics (Section 2.2) are simply produced by chance and are unreliable. However, because the detailed non-LTE calculations for smooth winds agree well with observed spectra for a variety of ions with different dependences on $\rho$, and because

[5]Note that at least for WR winds, clumping seems to be decisive because the analysis of the mass spectrum of the observed blobs implies a factor three overestimate in the mass loss derived from IR and radio observations (Moffat & Robert 1994), in rough agreement with the results from detailed line fits based on clumped wind models referred to in Section 5.1.

significant structure everywhere in the wind would disturb the ionization balance severely, this implication seems improbable.

Even if this were the case, however, the method to use the WLR of hot stars as an extragalactic distance indicator (see Section 6) would work because of the empirical calibration with stars at known distances as a function of spectral type and metallicity. On the other hand, all global quantities (Section 2.1) involving the mass-loss rate (linearly) would then have to be reduced by the square root of the effective clumping factor.



## 6. WINDS AND EXTRAGALACTIC STELLAR ASTRONOMY—OUTLOOK

Stellar winds with their broad and easily detectable spectral features distributed over the whole wavelength range from the UV to the IR are a gift of nature. With the new ground-based telescopes of the 8-m to 10-m class, stellar wind lines can easily be identified in medium-resolution spectra of blue supergiants individually observable out to distances of 20 Mpc (Kudritzki 2000) or in the integrated spectra of starburst regions in galaxies even much more distant, out to redshifts of $z \sim 4$ (Steidel et al 1996). Using the know-how obtained from the investigation of winds in the galaxies of our local group, these stellar wind features can provide unique information about young stellar populations, chemical composition, galactic evolution, and extragalactic distances.

Figure 12 shows the observed spectrum of the gravitationally lensed, highly redshifted starburst galaxy cB58 around the wavelength of the CIV resonance line, revealing a typical stellar wind P-Cygni profile blended by interstellar lines. As demonstrated by Pettini et al (2000), this line feature can be used to constrain the star formation process and metallicity. The authors conclude from the strength of the CIV feature that the metallicity must be smaller than solar. This conclusion is confirmed by the work of Walborn et al (1995) and Haser et al (1998), which indicates that metallicity has a substantial influence on the morphology of stellar wind lines.

Figure 13 shows the "modified" stellar wind momenta of A-supergiants in the galaxy and M31 as a function of absolute magnitude. As demonstrated by Kudritzki et al (1999), such a relationship can be used to determine extragalactic distances with an accuracy of about 0.1 mag in distance modulus out to the Virgo and Fornax clusters of galaxies. A-supergiants as the optically brightest "normal stars" with absolute magnitudes between $-9$ and $-8$ are ideal for this purpose. Their wind momenta can be determined solely by optical spectroscopy at $H_\alpha$. The quantitative analysis of the rest of the optical spectrum will yield effective temperature, gravity, chemical composition and—in conjunction with accurate photometry—reddening, and extinction so that an application of the wind momentum–luminosity relationship, properly calibrated as a function of metallicity in local group galaxies, will finally yield accurate distances.

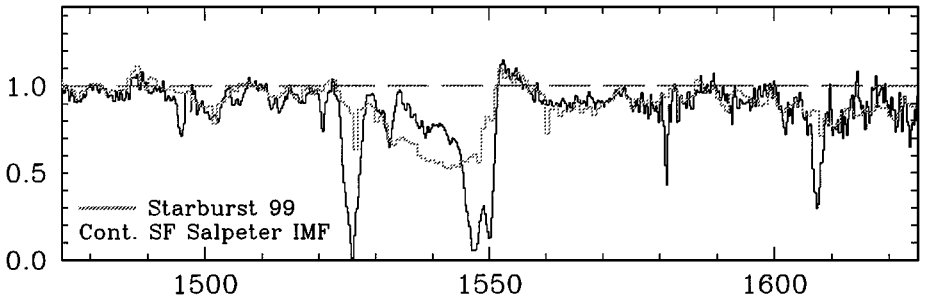


**Figure 12** Comparison between the observed rest-frame spectrum of the starburst galaxy cB58 (*black histogram*) at redshift $z = 2.72$ in the region of the Civ $\lambda$ 1549 stellar wind line with a spectral synthesis model, assuming continuous star formation and a Salpeter IMF. Note that the population synthesis code applied uses a library of observed spectra of galactic stars with abundances corresponding to the galactic disk at the solar neighborhood (see Leitherer et al 1999). From Pettini et al (2000).



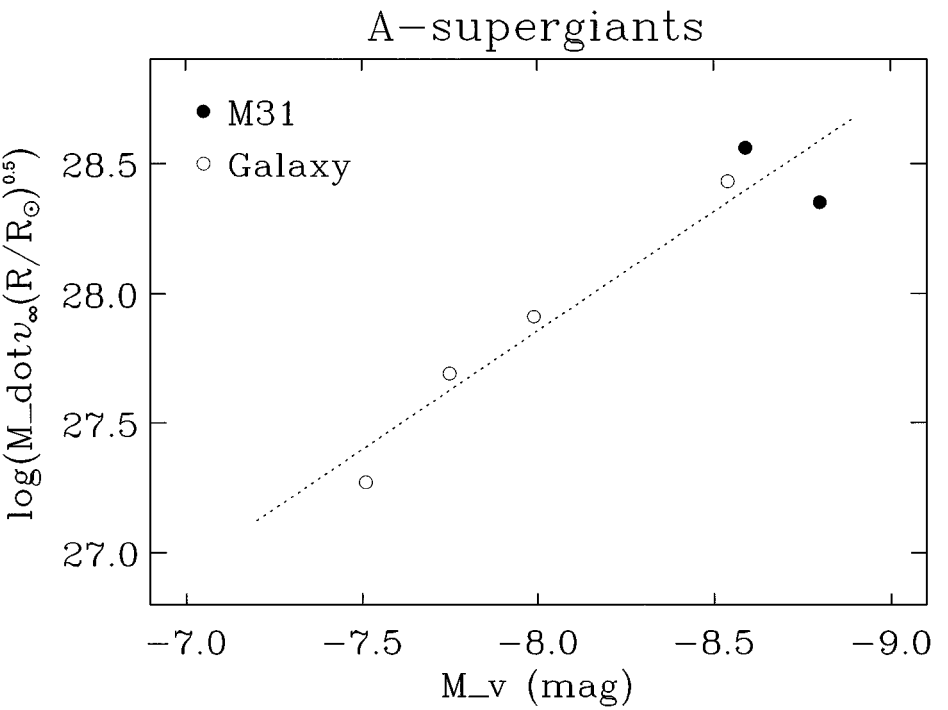


**Figure 13** Wind momenta of galactic and M31 A-supergiants as a function of absolute visual magnitude. The data of the M31 objects are from McCarthy et al (1997). (*dotted*) The linear regression obtained from all objects. From Kudritzki et al (1999).

## LITERATURE CITED


Abbott DC. 1978. *Ap. J.* 225:893
Abbott DC. 1979. *Proc. IAU Symp.* 83, p. 237
Abbott DC. 1980. *Ap. J.* 242:1183
Abbott DC. 1982. *Ap. J.* 259:282
Abbott DC, Bieging JH, Churchwell E, Cassinelli JP. 1980. *Ap. J.* 238:196
Abbott DC, Bieging JH, Churchwell E. 1981. *Ap. J.* 250:645
Abbott DC, Bieging JH, Churchwell E. 1984a. *Ap. J.* 280:671
Abbott DC, Telesco CM, Wolff SC. 1984b. *Ap. J.* 279:225
Achmad L, Lamers HJGLM, Pasquini L. 1997. *Astron. Astrophys.* 320:196
Altenhoff WJ, Thum C, Wendker H. 1994. *Astron. Astrophys.* 281:161
Babel J. 1995. *Astron. Astrophys.* 301:823
Babel J. 1996. *Astron. Astrophys.* 309:867
Barlow MJ, Cohen M. 1977. *Ap. J.* 213:737
Bates B, Gilheany S. 1990. *MNRAS* 243:320
Becker SR, Butler K. 1992. *Astron. Astrophys.* 265:647
Berghöfer TW, Schmitt JHMM. 1994. *Science* 265:1689
Berghöfer TW, Baade D, Schmitt JHMM, Kudritzki RP, Puls J, et al. 1996. *Astron. Astrophys.* 306:899
Berghöfer TW, Schmitt JHMM, Danner R, Cassinelli JP. 1997. *Astron. Astrophys.* 322:167
Bertout C, Leitherer C, Stahl O, Wolf B. 1985. *Astron. Astrophys. A* 144:87
Bieging JH, Abbott DC, Churchwell EB. 1989. *Ap. J.* 340:518
Bjorkman JE. 1999. *Proc. IAU Colloq. 169*, p. 121. Heidelberg: Springer-Verlag
Bjorkman JE, Cassinelli JP. 1993. *Ap. J.* 409:429
Blomme R, Runacres MC. 1997. *Astron. Astrophys.* 323:886
Bohannan B, Abbott DC, Voels SA, Hummer DG. 1986. *Ap. J.* 308:728
Carlberg RG. 1980. *Ap. J.* 241:1131
Cassinelli JP, Hartmann L. 1977. *Ap. J.* 212:488
Cassinelli JP, Swank JH. 1983. *Ap. J.* 271:681
Cassinelli JP, Cohen DH, MacFarlane JJ, Sanders WT, Welsh BY. 1994. *Ap. J.* 421:705
Castor JI. 1970. *MNRAS* 149:111
Castor JI, Simon T. 1983. *Ap. J.* 265:304
Castor JI, Abbott DC, Klein RI. 1975. *Ap. J.* 195:157
Chapman JM, Leitherer C, Koribalski B, Bouter R, Storey M. 1999. *Ap. J.* 518:890
Chen W, White RL. 1994. *Proc. Isle-aux-Coudre Workshop "Instability Variability Hot-Star Winds". Astrophys. Space Sci.* 221:259
Chlebowski T, Harnden FR, Sciortino S. 1989. *Ap. J.* 341:427
Cohen DH, Cooper RG, McFarlane JJ, Owocki SP, Cassinelli JP. 1996. *Ap. J.* 460:506
Cohen DH, Cassinelli JP, McFarlane JJ. 1997a. *Ap. J.* 487:867
Cohen DH, Cassinelli JP, Waldron WL. 1997b. *Ap. J.* 488:397
Conti PS, Blum RD. 1998. *Proc. 2nd Boulder-Munich Workshop. PASPC* 131:24
Contreras ME, Rodriguez LF, Gomez Y, Velazquez A. 1996. *Ap. J.* 469:329
Cooper RG, Owocki SP. 1992. *Proc. "Non-isotropic Variable Outflows from Stars" PASPC* 22:281
Cranmer SR, Owocki SP. 1995. *Ap. J.* 440:308
Cranmer SR, Owocki SP. 1996. *Ap. J.* 462:469
Crowther PA, Bohannan B, Pasquali A. 1998. *Proc. 2nd Boulder-Munich Workshop. PASPC* 131:38
de Koter A, Heap SR, Hubeny I. 1998. *Ap. J.* 509:879
Drake SA, Linsky JL. 1989. *Astron. J.* 98:1831
Drew JE. 1990. *Proc. 1st Boulder-Munich Workshop. PASPC* 7:218
Drew JE. 1998. *Proc. 2nd Boulder-Munich Workshop. PASPC* 131:14
Ebbets DC. 1982. *Ap. JS* 48:399
Eversberg T, Lepine S, Moffat AFJ. 1998. *Ap. J.* 494:799

Feldmeier A. 1995. *Astron. Astrophys.* 299:523
Feldmeier A. 1998. *Astron. Astrophys.* 332:245
Feldmeier A. 1999. *Proc. IAU Colloq. 169*, p. 285. Heidelberg: Springer-Verlag
Feldmeier A, Kudritzki RP, Palsa R, Pauldrach AWA, Puls J. 1997a. *Astron. Astrophys.* 320:899
Feldmeier A, Pauldrach AWA, Puls J. 1997b. *Astron. Astrophys.* 322:878
Figer DF, McLean IS, Najarro F. 1997. *Ap. J.* 486:1117
Figer DF, Najarro F, Morris M, McLean IS, Geballe TR, et al. 1998. *Ap. J.* 506:384
Friend DB, Abbott DC. 1986. *Ap. J.* 311:701
Fullerton AW. 1999. *Proc. IAU Colloq. 169*, p. 3. Heidelberg: Springer-Verlag
Fullerton AW, Gies DR, Bolton CT. 1992. *Ap. J.* 390:650
Fullerton AW, Gies DR, Bolton CT. 1996. *Ap. J.* 103:475
Fullerton AW, Massa, DL, Prinja RK, Owocki SP, Cranmer SR. 1997. *Astron. Astrophys.* 327:699
Gabler R, Gabler A, Kudritzki RP, Pauldrach AWA, Puls J. 1989. *Astron. Astrophys.* 226:162
Gabler A, Gabler R, Kudritzki RP, Puls J, Pauldrach A. 1990. *Proc. 1st Boulder-Munich Workshop. PASPC* 7:218
Gabler R, Kudritzki RP, Méndez RH. 1991. *Astron. Astrophys.* 245:587
Gabler R, Gabler A, Kudritzki RP, Méndez RH. 1992. *Astron. Astrophys.* 265:656
Gezari DY, Pitts PS, Schmitz M. 1999. *Catalog of Infrared Observations. Ed. 5.* ftp://cdsarc.u-strasbg.fr/pub/cats/II/225/
Grady CA, Snow TP, Timothy JG. 1983. *Ap. J.* 271:691
Grinin A. 1978. *Sov. Astron.* 14:113
Groenewegen MAT, Lamers HJGLM. 1989. *Astron. Astrophys.* 79:359
Groenewegen MAT, Lamers HJGLM, Pauldrach AWA. 1989. *Astron.Astrophys.* 221:78
Hamann WR. 1981a. *Astron. Astrophys.* 93: 353
Hamann WR. 1981b. *Astron. Astrophys.* 100:169
Hamann WR, Koesterke L. 1998. *Astron. Astrophys.* 335:1003
Hanson MM, Conti PS. 1994. *Ap. J. Lett.* 423:L139
Hanson MM, Conti PS, Rieke MJ. 1996. *Ap. J.* 107:281
Hanson MM, Howarth ID, Conti PS. 1997. *Ap. J.* 489:698
Hanson MM. 1998. *Proc. 2nd Boulder-Munich Workshop. PASPC* 131:1
Harnden FR, Branduardi G, Gorenstein P, Grindlay J, Rosner R, et al. 1979. *Ap. J. Lett.* 234:L51
Haser SM. 1995. *Spektroskopie heißer Sterne der Lokalen Gruppe im ultravioletten Spektralbereich*. PhD thesis. Ludwig-Maximilians Universität, München
Haser SM, Puls J, Kudritzki RP. 1994. *Space Sci. Rev.* 66:187
Haser SM, Lennon DJ, Kudritzki RP, Puls J, Pauldrach AWA, et al. 1995. *Astron. Astrophys.* 295:136
Haser SM, Pauldrach AWA, Lennon DJ, Kudritzki RP, Lennon M, et al. 1998. *Astron. Astrophys.* 330:285
Henrichs HF. 1984. *Proc. 4th Eur. IUE Conf., ESA-SP 218* , p. 43
Henrichs HF. 1991. *Proc. "Rapid Variability OB-Stars: Nature and Diagnostic Value". ESO Conf. Workshop Proc.* 36:199
Henrichs HF, Kaper L, Nichols JS. 1994. *Proc. IAU Symp. 162*, p. 517. Dordrecht: Kluwer
Henrichs HF, Kaper L, Zwarthoed GAA. 1988. *Proc. "A Decade UV Astron. IUE Satellite". ESA-SP 281*, 2:145
Herrero A, Kudritzki RP, Vilchez JM, Kunze D, Butler K, et al. 1992. *Astron. Astrophys.* 261:209
Herrero A, Corral LJ, Villamariz MR, Martin EL. 1999. *Astron. Astrophys.* 348:542
Herrero A, Puls J, Villamariz MR. 2000. *Astron. Astrophys.* 354:193
Hillier DJ. 1991. *Astron. Astrophys.* 247:455
Hillier DJ, Miller DL. 1998. *ApJ.* 496:407
Hillier DJ, Crowther PA, Najarro F, Fullerton AW. 1998. *Astron. Astrophys.* 340:438
Hillier DJ, Kudritzki RP, Pauldrach AWA,

Baade D, Cassinelli JP. 1993. *Astron. Astrophys.* 276:117

Howarth ID. 1992. *Proc. "Nonisotropic Variable Outflows Stars". PASPC* 22:155

Howarth ID, Brown AB. 1991. *Proc. IAU Symp. 143*, p. 289. Dordrecht: Kluwer

Howarth ID, Prinja RK. 1989. *Ap. J. Supp.* 69:527

Howarth ID, Prinja RK, Massa D. 1995. *Ap. J.* 452:L65

Howarth ID, Siebert KW, Hussain GA, Prinja RK. 1997. *MNRAS* 284:265

Hubeny I, Heap SR, Lanz T. 1998. *Proc. 2nd Boulder-Munich Workshop. PASPC* 131:108

Humphreys RM, McElroy DB. 1984. *Ap. J.* 284:565

Kaper L. 1993. *Wind variability in early-type stars.* PhD thesis. Univ. Amsterdam

Kaper L, Fullerton AW, eds. 1998. Cyclical variability in stellar winds. *ESO Astrophys. Symp.* Heidelberg: Springer-Verlag

Kaper L, Henrichs HF. 1994. *Proc. Isle-aux-Coudre Workshop* "Instability Variability Hot-Star Winds". *Astrophys. Space Sci.* 221:115

Kaper L, Henrichs HF, Fullerton AW, Ando H, Bjorkman KS, et al. 1997. *Astron. Astrophys.* 327:281

Kaper L, Henrichs HF, Nichols JS, Telting JH. 1999. *Astron. Astrophys.* 344:231

Kaufer A, Stahl O, Wolf B, Gäng T, Gummersbach CA, et al. 1996. *Astron. Astrophys.* 305:887

Klein RI, Castor JI. 1978. *Ap. J.* 220:902

Kudritzki RP. 1979. *Proc. 22nd Liege Int. Symp.*, p. 295

Kudritzki RP. 1980. *Astron. Astrophys.* 85: 174

Kudritzki RP. 1988. *18th Adv. Course Swiss Soc. Astrophys. Astron.*, Saas-Fee Courses, Geneva Obs., 1

Kudritzki RP. 1998. Quantitative spectroscopy of the brightest blue supergiant stars in galaxies. *Proc. 8th Canary Winter Sch.*, p. 149. Cambridge Univ. Press

Kudritzki RP. 1999a. *Proc. IAU Colloq. 169*, p. 405. Heidelberg: Springer-Verlag

Kudritzki RP. 1999b. *Proc. STScI Symp. "Unsolved Problems of Stellar Evolution"*, In press

Kudritzki RP. 2000. *VLT Opening Symp. ESO*. In press

Kudritzki RP, Simon KP, Hamann WR. 1983. *Astron. Astrophys.* 118:254

Kudritzki RP, Pauldrach AWA, Puls J. 1987. *Astron. Astrophys.* 173:293

Kudritzki RP, Pauldrach A, Puls J, Abbott DC. 1989. *Astron. Astrophys.* 219:205

Kudritzki RP, Hummer DG, Pauldrach AWA, Puls J, Najarro J, et al. 1992. *Astron. Astrophys.* 257:655

Kudritzki RP, Lennon DJ, Puls J. 1995. *Proc. ESO Workshop"Science VLT"*, p. 246. Heidelberg: Springer-Verlag

Kudritzki RP, Palsa R, Feldmeier A, Puls J, Pauldrach AWA. 1996. *Proc. "Roentgenstrahlung from the Universe". MPE Rep.* 263:9

Kudritzki RP, Méndez RH, Puls J, McCarthy JK. 1997. *Proc. IAU Symp. 180*, p. 64

Kudritzki RP, Springmann U, Puls J, Pauldrach AWA, Lennon M. 1998. *Proc. 2nd Boulder-Munich Workshop. PASPC* 131:299

Kudritzki RP, Puls J, Lennon DJ, Venn KA, Reetz J, et al. 1999. *Astron. Astrophys.* 350:970

Lamers HJGLM, Waters LBFM. 1984a. *Astron. Astrophys.* 136:37

Lamers HJGLM, Waters LBFM. 1984b. *Astron. Astrophys. A* 138:25

Lamers HJGLM, Pauldrach AWA. 1991. *Astron. Astrophys. A* 244:L5

Lamers HJGLM, Leitherer C. 1993. *Ap. J.* 412:771

Lamers HJGLM, Gathier R, Snow TP. 1982. *Ap. J.* 258:186

Lamers HJGLM, Waters LBFM, Wesselius PR. 1984. *Astron. Astrophys.* 134:L17

Lamers HJGLM, Cerruti-Sola M, Perinotto M. 1987. *Ap. J.* 314:726

Lamers HJGLM, Snow TP, Lindholm DM. 1995. *Ap. J.* 455:269

Lamers HJGLM, Najarro F, Kudritzki RP, Morris PW, Voors RHM, et al. 1996. *Astron. Astrophys.* 315:L225

Lamers HJGLM, Haser SM, de Koter A, Leitherer C. 1999a. *Ap. J.* 516:872
Lamers HJGLM, Vink JS, de Koter A, Cassinelli JP. 1999b. *Proc. IAU Colloq. 169*, p. 159. Heidelberg: Springer-Verlag
Langer N, Heger A. 1998. *Proc. 2nd Boulder-Munich Workshop. PASPC* 131:76
Langer N, Hamann WR, Lennon M, Najarro F, Pauldrach AWA, et al. 1994. *Astron. Astrophys.* 290:819
Lanz T, de Koter A, Hubeny I, Heap SR. 1996. *Ap. J.* 465:359
Leitherer C. 1988. *Ap. J.* 326:356
Leitherer C. 1998. *Proc. 8th Canary Winter Sch.* p. 527. Cambridge Univ. Press
Leitherer C, Robert C. 1991. *Ap. J.* 377:629
Leitherer C, Robert C, Drissen L. 1992. *Ap. J.* 401:596
Leitherer C, Chapman JM, Koribalski B. 1995. *Ap. J.* 450:289
Leitherer C, Schaerer D, Goldader JD, Gonzalez RM, Robert C, et al. 1999. *Ap. J.* 123:3
Lennon DJ, Kudritzki RP, Becker ST, Butler K, Eber F, et al. 1991. *Astron. Astrophys.* 252:498
Lucy LB, White RL. 1980. *Ap. J.* 241:300
Lucy LB. 1982a. *Ap. J.* 255:278
Lucy LB. 1982b. *Ap. J.* 255:286
Lucy LB. 1983. *Ap. J.* 274:372
Lucy LB. 1984. *Ap. J.* 284:351
Lupie OL, Nordsieck KH. 1987. *Astron. J* 93:214
MacFarlane JJ, Cassinelli JP. 1989. *Ap. J.* 347:1090
MacFarlane JJ, Waldron WL, Corcoran MF, Wolff MJ, Wang P, et al. 1993. *Ap. J.* 419:813
MacGregor KB, Hartmann L, Raymond JC. 1979. *Ap. J.* 231:514
Maeder A. 1998. *Proc. 2nd Boulder-Munich Workshop. PASPC* 131:85
Maeder A. 1999. *Astron. Astrophys.* 347:185
Massa D, Fullerton AW, Nichols JS, Owocki SP, Prinja RK, et al. 1995. *Ap. J.* 452:L53
McCarthy JK, Lennon DJ, Venn KA, Kudritzki RP, Puls J, et al. 1995. *Ap. J. Lett.* 455:L35
McCarthy JK, Kudritzki RP, Lennon DJ, Venn KA, Puls J. 1997. *Ap. J.* 482:757
McCarthy JK, Venn KA, Lennon DJ, Kudritzki RP, Puls J. 1998. *Proc. 2nd Boulder-Munich Workshop. PASPC* 131:197
McErlean ND, Lennon DJ, Dufton PL. 1998 *Astron. Astrophys.* 329:613
McErlean ND, Lennon DJ, Dufton PL. 1999 *Astron. Astrophys.*, In press
Méndez RH, Kudritzki RP, Herrero A, Husfeld D, Groth HG. 1988. *Astron. Astrophys.* 190:113
Meynet G. 1998. *Proc. 2nd Boulder-Munich Workshop. PASPC* 131:96
Mihalas D. 1978. *Stellar Atmospheres.* Freeman: San Francisco. 2nd ed.
Moffat AFJ, Robert C. 1994. *Ap. J.* 421:310
Moffat AFJ, Owocki SP, Fullerton AW, St-Louis N, eds. 1994. *Proc. Isle-aux-Coudre Workshop "Instability and Variability of Hot-Star Winds". Astrophys. Space Sci.* 221:467
Mullan DJ. 1984. *Ap. J.* 283:303
Mullan DJ. 1986. *Astron. Astrophys.* 165: 157
Najarro F, Hillier JD, Kudritzki RP, Krabbe A, Genzel R, et al. 1994. *Astron. Astrophys.* 285:573
Najarro F, Kudritzki RP, Cassinelli JP, Stahl O, Hillier DJ. 1996. *Astron. Astrophys.* 306:892
Najarro F, Hillier DJ, Stahl O. 1997a. *Astron. Astrophys.* 326:1117
Najarro F, Krabbe A, Genzel R, Lutz D, Kudritzki RP, et al. 1997b. *Astron. Astrophys.* 325:700
Najarro F, Kudritzki RP, Hillier DJ, Lamers HJGLM, Voors RHM, et al. 1998. *Proc. 2nd Boulder-Munich Workshop. PASPC* 131:57
Napiwotzki R, Green PJ, Saffer RA. 1999. *Ap. J.* 517:399
Olson GL. 1982. *Ap. J.* 255:267
Owocki SP. 1991. *Proc. "Stellar Atmospheres: Beyond Classical Models". NATO ASI Ser. C* 341:235. Dordrecht: Kluwer
Owocki SP. 1992. *Proc. "The Atmospheres of Early-Type Stars"*, p. 393. Berlin: Springer-Verlag
Owocki SP. 1994. *Proc. Isle-aux-Coudre Workshop "Instability and Variability of Hot-Star Winds". Astrophys. and Space Sci.* 221:3

Owocki SP. 1999. *Proc. IAU Colloq. 169*, p. 294. Heidelberg: Springer-Verlag
Owocki SP, Rybicki GB. 1984. *Ap. J.* 284:337
Owocki SP, Rybicki GB. 1985. *Ap. J.* 299:265
Owocki SP, Puls J. 1996. *Ap. J.* 462:894
Owocki SP, Puls J. 1999. *Ap. J.* 510:355
Owocki SP, Cohen DH. 1999. *Ap. J.* 520:833
Owocki SP, Castor JI, Rybicki GB. 1988. *Ap. J.* 335:914
Owocki SP, Cranmer SR, Fullerton AW. 1995. *Ap. J.* 453:L37
Owocki SP, Cranmer SR, Blondin JM. 1994. *Ap. J.* 424:887
Owocki SP, Cranmer SR, Gayley KG. 1996. *Ap. J.* 472:L1150
Owocki SP, Cranmer SR, Gayley KG. 1998a. *Proc. Workshop "B[e] Stars". Astrophys. and Space Sci.* 233:205. Dordrecht: Kluwer
Owocki SP, Gayley KG, Cranmer SR. 1998b. *Proc. 2nd Boulder-Munich Workshop*. *PASPC* 131:237
Pallavicini R, Golub L, Rosner R, Vaiana GS, Ayres T, et al. 1981. *Ap. J.* 248: 279
Panagia N, Felli M. 1975. *Astron. Astrophys.* 39:1
Pauldrach AWA, Puls J. 1990. *Astron. Astrophys.* 237:409
Pauldrach AWA, Puls J, Kudritzki RP. 1986. *Astron. Astrophys.* 164:86
Pauldrach AWA, Puls J, Kudritzki RP, Méndez RH, Heap SR. 1989. *Astron. Astrophys.* 207:123
Pauldrach AWA, Puls J, Kudritzki RP, Butler K. 1990. *Astron. Astrophys.* 228:125
Pauldrach, AWA, Kudritzki RP, Puls J, Butler K, Hunsinger J. 1994. *Astron. Astrophys.* 283:525
Pauldrach AWA, Lennon M, Hoffmann TL, Sellmaier F, Kudritzki RP, Puls J. 1998. *Proc. 2nd Boulder-Munich Workshop*. *PASPC* 131:258
Perinotto M. 1993. *Proc. IAU Symp. 155*, p. 57. Dordrecht: Kluwer
Petrenz P. 1999. *Selbstkonsistente Modelle strahlungsdruckgetriebener Winde heisser Sterne unter Mitberücksichtigung der Rotation*. PhD thesis. Ludwig-Maximilians Universität, München
Petrenz P, Puls J. 1996. *Astron. Astrophys.* 312:195
Pettini M, Steidel CC, Adelberger KL, Dickinson M, Giavalisco M. 2000 *Ap. J.*, 528:96
Pollock AMT. 1989. *Proc. Int. Sch. Workshop on Reconnect. in Space Plasma*, 2:309
Prinja RK. 1988. *MNRAS* 231:21P
Prinja RK. 1992. *Proc. "Nonisotropic and Variable Outflows Stars"*. *PASPC* 22:167
Prinja RK, Howarth ID. 1986. *Ap. JS* 61:357
Prinja RK, Howarth ID. 1988. *MNRAS* 233: 123
Prinja RK, Smith LJ. 1992. *Astron. Astrophys.* 266:377
Prinja RK, Crowther PA. 1998. *MNRAS* 300:828
Prinja RK, Massa DL. 1998. *Proc. 2nd Boulder-Munich Workshop*. *PASPC* 131:218
Prinja RK, Howarth ID, Henrichs HF. 1987. *Ap. J.* 317:389
Prinja RK, Barlow MJ, Howarth ID. 1990. *Ap. J.* 361:607
Prinja RK, Balona LA, Bolton CT, Crowe RA, Fieldus MS, et al. 1992. *Ap. J.* 390:266
Prinja RK, Massa DL, Fullerton AW. 1995. *Ap. J.* 452:L61
Puls J. 1987. *Astron. Astrophys.* 184:227
Puls J. 1993. *Winde heißer massereicher Sterne—Theoretische Ansätze und diagnostische Methoden*. Habilitation thesis. *Ludwig-Maximilians Universität, München*
Puls J, Owocki SP, Fullerton AW. 1993a. *Astron. Astrophys.* 279:457
Puls J, Pauldrach AWA, Kudritzki RP, Owocki SP, Najarro F. 1993b. *Rev. in Mod. Astron.* 6:271.
Puls J, Feldmeier A, Springmann UWE, Owocki SP, Fullerton AW. 1994. *Proc. Isle-aux-Coudre Workshop "Instability and Variability of Hot-Star Winds"*. *Astrophys. Space Sci.* 221:409
Puls J, Kudritzki RP, Herrero A, Pauldrach AWA, Haser SM, et al. 1996. *Astron. Astrophys.* 305:171
Puls J, Kudritzki RP, Santolaya-Rey AE,

Herrero A, Owocki SP, et al. 1998. *Proc. 2nd Boulder-Munich Workshop*. *PASPC* 131:245
Puls J, Petrenz P, Owocki SP. 1999 *Proc. IAU Colloq. 169*, p. 131. Heidelberg: Springer-Verlag
Puls J, Springmann U, Lennon M. 2000 *Astron. Astrophys.* 141:23
Runacres MC, Blomme R. 1996. *Astron. Astrophys.* 309:544
Santolaya-Rey AE, Puls J, Herrero A. 1997. *Astron. Astrophys.* 323:488
Schaerer D, Schmutz W. 1994. *Astron. Astrophys.* 288:231
Schaerer D, de Koter A. 1997. *Astron. Astrophys.* 322:598
Schmutz W. 1997. *Astron. Astrophys.* 321:268
Schönberber D. 1983. *Ap. J.* 272:708
Scuderi S, Bonanno G, Di Benedetto R, Spadaro D, Panagia N. 1992. *Ap. J.* 392:201
Scuderi S, Panagia N, Stanghellini C, Trigilio C, Umana G. 1998. *Astron. Astrophys.* 332: 251
Sellmaier F, Puls J, Kudritzki RP, Gabler A, Gabler R, et al. 1993. *Astron. Astrophys.* 273:533
Seward FD, Forman WR, Giacconi R, Griffiths RE, Harnden FR, et al. 1979. *Ap. J. Lett.* 234:L55
Simon KP, Jonas G, Kudritzki RP, Rahe J. 1983. *Astron. Astrophys.* 125:34
Skinner CJ, Becker RH, White RL, Exter KM, Barlow MJ, Davis RJ. 1998. *MNRAS* 296: 669
Smith KC, Howarth ID. 1998. *MNRAS* 299:1146
Sobolev VV. 1957. *Sov. Astron. Astrophys. J.* 1:678
Springmann UWE, Pauldrach, AWA. 1992. *Astron. Astrophys.* 262:515
Springmann U, Puls J. 1998. *Proc. 2nd Boulder-Munich Workshop*. *PASPC* 131:286
Stahl O, Wolf B, Aab O, Smolinski J. 1991. *Astron. Astrophys.* 252:693
Steidel CC, Giavalisco M, Pettini M, Dickinson M, Adelberger KL. 1996. *Ap. J. Lett.* 462:L17
Stevens IR. 1995. *MNRAS* 277:163
Tanzi EG, Tarenghi M, Panagia N. 1981. *Proc. 59th Colloq. Trieste*, p. 51. Dordrecht:Reidel
Taresch G, Kudritzki RP, Hurwitz M, Bowyer S, Pauldrach AWA, et al. 1997. *Astron. Astrophys.* 321:531
Venn KA. 1995. *Ap. J.* 449:839
Venn KA. 1999. *Ap. J.* 518:405
Vink JS, de Koter A, Lamers HJGLM. 1999. *Astron. Astrophys.* 350:18
Voels SA, Bohannon B, Abbott DC, Hummer DG. 1989. *Ap. J.* 340:1073
Walborn NR, Panek RJ. 1984. *Ap. J. Lett.* 280:L27
Walborn NR, Noichols-Bohlin J, Panek RJ. 1985. *International Ultraviolet Explorer Atlas of O-Type Spectra From 1200 to 1900 Å. NASA Ref. Publ.* 1155.
Walborn NR Lennon DJ, Haser SM, Kudritzki RP, Voels SA. 1995. *PASP* 107:104
Waters LBFM, Lamers HJGLM. 1984. *Astron. Astrophys.* 57:327
Waters LBFM, Wesselius PR. 1986. *Astron. Astrophys.* 155:104
Wendker HJ. 1987. *Astron. Astrophys.* 69:87
White RL, Becker RH. 1982. *Ap. J.* 262: 657
White RL, Becker RH. 1983. *Ap. J. Lett.* 272:L19
Wolf B, Stahl O, Fullerton AW. eds. 1999. *Proc. IAU Colloq. 169*, p. 169. Heidelberg: Springer-Verlag
Wood PR, Faulkner DJ. 1986. *Ap. J.* 307:659
Wright AE, Barlow MJ. 1975. *MNRAS* 170: 41
Zickgraf FJ. 1999. *Proc. IAU Colloq.* 169, p. 40 Heidelberg: Springer-Verlag

*Annual Review of Astronomy and Astrophysics*
*Volume 38, 2000*

# CONTENTS